Journal of Medicinal Chemistry

pubs.acs.org/jmc

Article

Interfering with the Tumor−Immune Interface: Making Way for Triazine-Based Small Molecules as Novel PD-L1 Inhibitors

Pasquale Russomanno, Giulia Assoni, Jussara Amato, Vincenzo Maria D'Amore, Riccardo Scaglia, Diego Brancaccio, Martina Pedrini, Giovanna Polcaro, Valeria La Pietra, Paolo Orlando, Marianna Falzoni, Linda Cerofolini, Stefano Giuntini, Marco Fragai, Bruno Pagano, Greta Donati, Ettore Novellino, Cristina Quintavalle, Gerolama Condorelli, Francesco Sabbatino,* Pierfausto Seneci,* Daniela Arosio,* Stefano Pepe, and Luciana Marinelli*

Cite This: https://doi.org/10.1021/acs.jmedchem.1c01409

Read Online

ACCESS | Metrics & More | Article Recommendations | Supporting Information

ABSTRACT: The inhibition of the PD-1/PD-L1 axis by monoclonal antibodies has achieved remarkable success in treating a growing number of cancers. However, a novel class of small organic molecules, with BMS-202 (**1**) as the lead, is emerging as direct PD-L1 inhibitors. Herein, we report a series of 2,4,6-tri- and 2,4-disubstituted 1,3,5-triazines, which were synthesized and assayed for their PD-L1 binding by NMR and homogeneous time-resolved fluorescence. Among them, compound **10** demonstrated to strongly bind with the PD-L1 protein and challenged it in a co-culture of PD-L1, expressing that cancer cells (PC9 and HCC827 cells) and peripheral blood mononuclear cells enhanced antitumor immune activity of the latter. Compound **10** significantly increased interferon γ release and apoptotic induction of cancer cells, with low cytotoxicity in healthy cells when compared to **1**, thus paving the way for subsequent preclinical optimization and medical applications.

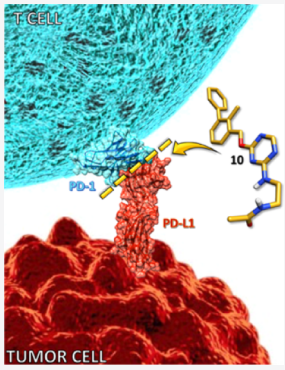

■ INTRODUCTION

An intimate relationship between cancer and immune function was first proposed more than a century ago by Rudolf Virchow, who observed the prevalence of leukocytes in tumors.[1] Since then, and for at least the following 100 years, limited advancements were reported in the comprehension of the biological pathways activated upon interaction between the cancer cells and the immune system. Although much remains to be understood, it is clear that malignant cells evade the attack by the immune system and that this "tolerance" is obtained by multiple mechanisms involving immunosuppressive cytokines or the so-called immune checkpoint receptors (ICRs). Both the above-mentioned molecular mechanisms contribute to local remodeling of the tumor microenvironment (TME) and in secondary organs predisposing "premetastatic niches", where a fertile soil for immune escape and cancer growth is guaranteed. Recent studies even suggest that exosomes released by the tumor play a key role to shuttle down the antitumor immunity systemically.[2]

Among ICRs, cytotoxic T-lymphocyte protein 4, PD-1 (programmed cell death protein 1), indoleamine 2,3-dioxygenase, T-cell immunoglobulin and mucin domain-containing protein 3, and lymphocyte-activation gene 3 have garnered the most attention so far.[3] Specifically, PD-1 is a cell−surface receptor expressed by $CD8^+$ T cells on activation, during priming or expansion. It is now known that TME can prompt the overexpression of the PD-1 receptor on infiltrated T cells, while its physiological ligand PD-L1 is overexpressed on tumor cell membranes and on deriving extracellular vesicles, mostly as exosomes.[2] Recognition and binding of cellular PD-1 and cellular or exosomal PD-L1 (ExoPD-L1) generate an inhibitory signal that attenuates the activity of T cells in cancer patients, thus inhibiting antitumor immunity and causing T-cell exhaustion. The "exhaustion" of effector T (Teff) cells was found to be an important negative feedback loop that ensures immune homeostasis against cancer. In this respect, it has been demonstrated that ExoPD-L1 facilitate tumor growth, both *in vitro* and *in vivo*,[2,4] and that its levels are associated with disease activity, stage, and lymph node status, and finally with poor prognosis in many cancer types.[5,6] In this perspective, the PD-1/PD-L1 axis can be impaired by targeting either cellular PD-1 or cellular/exosomal PD-L1 with antibodies. In fact, two PD-1 specific mAbs, Pembrolizumab (Keytruda by Merck)[7] and Nivolumab [Opdivo by Bristol-Myers Squibb (BMS)],[8] provided the first clinical pieces of proof that cancer can be

Received: August 8, 2021

Chart 1. Pharmacophoric Model and Chemical Structures of Representative Small Molecules as Direct Inhibitors of PD-1/PD-L1 Binding, along with Our Newly Developed Compounds.

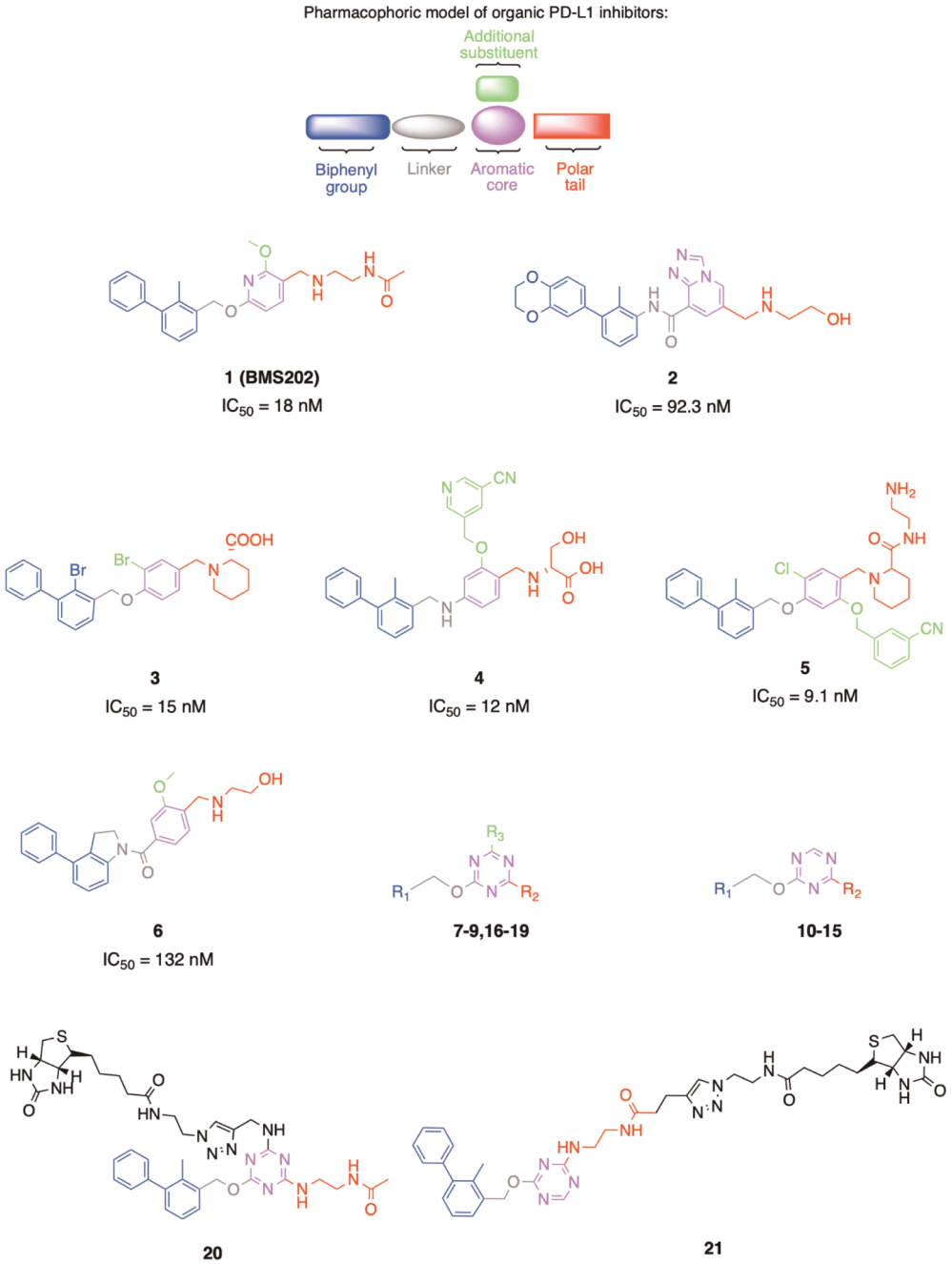

addressed by the modulation of the immune response.[9] Following this success, PD-L1-specific antibodies (atezolizumab, cemiplimab, durvalumab, atezolizumab, and avelumab) entered the market too.[10,11] At present, anti-PD-1/anti-PD-L1 antibodies have been tested in more than 1000 clinical trials and approved for several cancer types, including melanoma, renal cell carcinoma, Hodgkin's lymphoma, bladder cancer, head and neck squamous cell carcinoma, and, more recently, non-small cell lung cancer (NSCLC).[12,13] However, despite their remarkable success in selected patients, antibodies have specific, well-known drawbacks as therapeutics, including but not limited to high production costs, lack of oral bioavailability, long circulating half-life, poor tissue and tumor penetrating capacity,[14] and immune-related adverse events.[15]

In an attempt to overcome some of these problems, a number of small molecules, such as macrocyclic peptides and organic compounds targeting PD-L1, have been reported, initially only in patent applications.[16−37] BMS first patented a series of biphenyl ether-based compounds (eg., **1**, also known as BMS-202, see Chart 1) able to disrupt the PD-1/PD-L1 complex with an IC_{50} ranging between 1 and 300 nM.[17,18] Only in 2015, the structural basis for the human PD-1/PD-L1 protein−protein interaction was unraveled by X-ray crystallography.[38] Later on, structures of PD-L1 in complex with antibodies, peptide macrocycles, and small organic compounds (eg., **1**) have been released too,[22,39,40] revealing that ligands can recognize partially overlapping regions on the PD-L1 surface.[22,25,41−43] However, the flat and hydrophobic binding surface of PD-L1 made it

https://doi.org/10.1021/acs.jmedchem.1c01409
J. Med. Chem. XXXX, XXX, XXX−XXX

Scheme 1. Synthesis of 2,4,6-Trisubstituted Cyanobenzyl Triazines 7−9

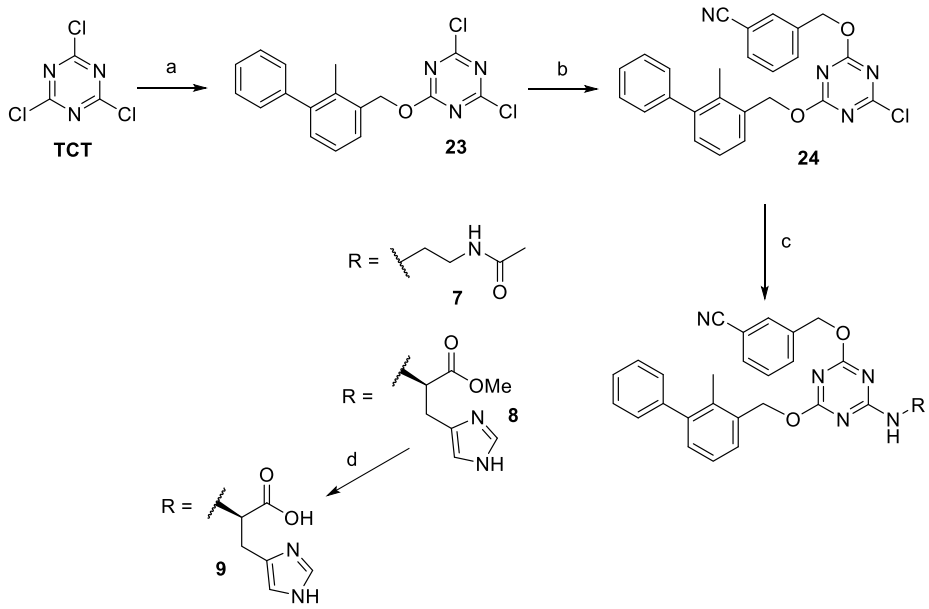

a) (2-methyl-[1,1'-biphenyl]-3-yl)methanol, DIPEA, dry DCM, -20°C to rt, 2.5h, **70%**; b) 3-(hydroxymethyl)benzonitrile, DIPEA, dry DCM, rt, 48h, **70%**; c) N-acetyl ethylenediamine or L-histidine methylester, DIPEA, dry CH_3CN, 70°C, 5-16h, **72%** (**7**), **62%** (**8**); d) LiOH H_2O, 3:1 THF/H_2O, rt, 3h, **60%**.

immediately clear that the rational design of small inhibitors would have been all but easy. In this scenario, the discovery of **1** has represented a precious starting point for ligand-based design or "me too" strategies that led to the discovery of compounds **2**-**6** (Chart 1).[29−31,33,35]

Thus, a number of studies aiming at the evaluation of *in vivo* anticancer properties of biphenyl ether-based compounds are quickly arising. Some studies are of doubtful value with respect to PD-L1-dependent effects in mice, as **1** has been used in animal models expressing mouse PD1/PD-L1[44] and evidence exists that **1** does not bind mouse PD-L1,[45] thus some off-target should be responsible for the anticancer results. Other studies seem more meaningful and promising in this respect. For example, compounds **4** and **5** were challenged in an immune checkpoint-humanized mouse model, demonstrating to be highly effective in suppressing tumor growth,[30,31] thus prompting further development of biphenyl ether- and amine-based compounds. In fact, development of structurally new PD-L1 small ligands would be of utmost importance for a complete understanding of the full potential of small-molecule PD1/PD-L1 inhibitors either as therapeutics or as diagnostic tools. Being aware that the biphenyl ether in compounds **1**−**6** is the main driving group for PD-L1 surface binding[33] that a central aromatic core is necessary to oppositely orient the two main PD-L1 interacting chains (e.g., 1,4 diamino-acetyl and biphenyl ether-based chains in compound **1**, Chart 1) and that para and meta substitutions on the central core seem both to be acceptable (see structures 1 and 2 in Chart 1 as an example); we looked for an accessible and synthetically flexible aryl scaffold replacement. Herein, a series of 2,4,6-tri- and 2,4-disubstituted 1,3,5-triazines were reported. Specifically, the novel compounds were synthesized, qualitatively tested by one-dimensional (1D) ^{1}H NMR, and then quantitatively tested through a homogeneous time-resolved fluorescence (HTRF) binding assay that furnished an IC_{50} for each binder found through NMR. Disubstituted triazine **10** was identified as the most potent early lead and through NMR was shown to specifically bind PD-L1 but not to PD-1. NMR assays were also performed on PD-L1-containing exosomes, once more confirming the binding event.

Finally, two biotinylated, either trisubstituted (**20**) or disubstituted (**21**) derivatives, were synthesized and used in immunofluorescent double-staining experiments on four different cell lines expressing diverse levels of PD-L1 to confirm the capability of our triazine-based compounds to also bind to PD-L1 on cell membranes, besides free or exosomal protein copies.

Activated PBM cells co-cultured with PC9 or HCC827 cancer cells were set up to assess the immunomodulatory activity and the functional significance of PD-L1 inhibition by **10**. IFNγ release by co-cultured activated PBM cells in the presence and in the absence of potent PD-L1 inhibitors (**1** and **10**) was also evaluated. Finally, a computer-aided rationalization of early structure−activity relationships (SARs) developed through triazine-based compounds **7**−**19** was established. The structural insights into the binding mode of **10** on the PD-L1 surface, together with a comparison with the binding mode for standard **1**, surely will represent another piece to the puzzle of PD-L1/small-molecule interactions.

■ RESULTS AND DISCUSSION

Ligand Design and Chemistry. Based on core synthetic versatility, and on our synthetic expertise, among a number of possible central scaffolds potentially supporting the 1,4 diamino-acetyl and the biphenyl ether-based chains either in para (e.g., the 5,6,7,8-tetrahydro-[1,2,4]triazolo[4,3-*a*]pyrazine or an indole) or in meta position (e.g., 1,3,5-triazine ring), we have chosen the latter 1,3,5-triazine ring, a known privileged structure in medicinal chemistry.

To this regard, trichloro (cyanuric chloride, TCT) and dichloro triazines (DCT) are cheap and largely used reagents due to the different reactivity-sequential substitution of each chlorine atom toward nucleophiles. In particular, the displacement of each chlorine atom in TCT and DCT by various

https://doi.org/10.1021/acs.jmedchem.1c01409
J. Med. Chem. XXXX, XXX, XXX−XXX

nucleophiles leads to mono-, di-, and tri-substituted 1,3,5-triazines. Stepwise chlorine substitution with O-, S-, and N-nucleophiles can be controlled by temperature and nucleophile strength; an empirical rule for TCT is that the first chlorine substitution should occur below or around 0 °C, the second around room temperature, and the last substitution above 60 °C;[46] as to DCT, two sequential substitutions typically entail room temperature and around 60 °C.

Herein, aware that the biphenyl ether or amine moiety in compounds **1**−**6** is the driving group for PD-L1 surface binding,[33] we synthesized a small array of triazines **7**−**21** (Chart 1) preserving this key pattern and substituting the polar chain with a few polar groups that were demonstrated to be activity compliant in BMS202 patents.[17,18] Specifically, we explored the influence of histidine-based (**8**, **9**, **11**, and **12**), varying chain lengths ending with an acetamide (**7**, **10**, and **13**), terminal direct (**14**), or inverse sulfonamide (**15**), and a biotin-decorated triazole diamide (**20**) for biological purposes (see further on). A third substituent, when present, was a cyanobenzyl ether in triazines **7**−**9**, according to known PD-L1 inhibitors in papers and patents.[17,18] Alternatively, to enlarge the SARs, we explored the effect of smaller third substituents such as chlorine (**16**), a hydroxyl (**17**), a **1**-like methyl ether (**18**), a methyl group (**19**), and a biotinylated triazole amide (**21**).

The following synthetic procedures for triazines **7**−**21** are reported and sub-divided in groups depending on synthetic similarity. Please note that the order of nucleophilic substitutions on R_1, R_2, and, for trisubstituted triazines, R_3 may vary in different strategies, depending on the reactivity of each substituent.

Synthesis of 2,4,6-Trisubstituted Cyanobenzyl Triazines 7−9. The first step in the synthesis of 2,4,6-trisubstituted cyanobenzyl triazines **7**−**9** entailed the introduction of a biphenyl ether substituent onto the triazine core (step **a**, Scheme 1). Namely, a nucleophilic substitution between (2-methyl-[1,1′-biphenyl]-3-yl)methanol and TCT in the presence of an organic base was carried out by slowly increasing the temperature from −20 °C to room temperature, in order to minimize the risk of a double nucleophilic addition. The reaction proceeded smoothly and rapidly, affording the desired dichloro biphenyl ether triazine **23** in good yields. Intermediate **23** was subsequently reacted in a second substitution (step **b**) with (hydroxymethyl)benzonitrile, employing similarly mild reaction conditions but for a significantly longer reaction time. The desired chloro diether triazine **24** was obtained in good yields. A third substitution (step **c**) entailed the use of more reactive *N*-nucleophiles (*N*-acetyl ethylenediamine—target amide **7**, L-histidine methyl ester—target ester **8**) in stronger experimental conditions; both tri-substituted triazines **7** and **8** were obtained in good yields. Finally, standard basic hydrolysis of ester **8** led to target free carboxylate triazine **9** (step **d**, Scheme 1).

Synthesis of 2,4-Disubstituted Triazines 10−12. The synthetic strategy envisaged for the preparation of 2,4-disubstituted triazines **10**−**12** (Scheme 2) is similar to the one just described for targets **7**−**9** in Scheme 1.

Namely, the first nucleophilic substitution between (2-methyl-[1,1′-biphenyl]-3-yl)methanol and 2,4-dichlorotriazine was started at −20 °C, with gradual warming to room temperature (step **a**, Scheme 2). The desired chlorobiphenyl ether triazine **25** was obtained in moderate yields after a longer reaction time than seen for intermediate **23** (step **a**, Scheme 1); preliminary optimization attempts by forcing the reaction

Scheme 2. Synthesis of 2,4-Disubstituted Triazines 10−12

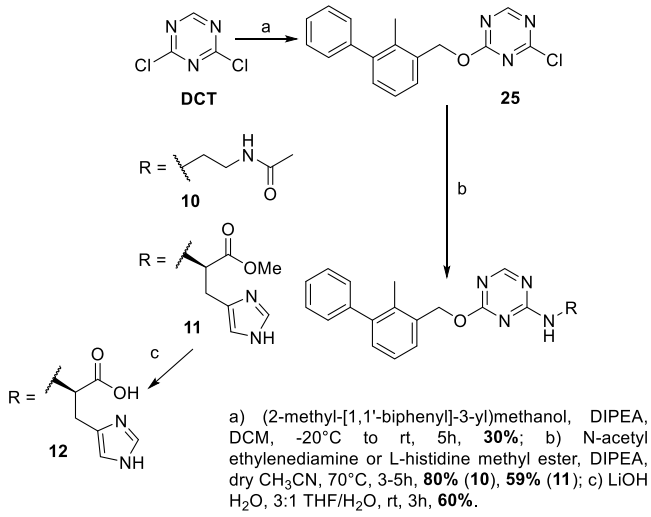

conditions were unsuccessful, mostly due to the formation of complex reaction mixtures. The introduction of *N*-acetyl ethylenediamine—**10** -or L-histidine methylester—**11**—in a second substitution (step **b**) was carried out with the same experimental protocol used for tri-substituted triazines in Scheme 1 (compare with step **c**, Scheme 1), obtaining both targets with similar yields. Triazine **11** was then submitted to standard basic hydrolysis (step **c**, Scheme 2), producing target-free carboxylate **12** in moderate overall yields.

Polar Chain Modification: Synthesis of 2,4-Disubstituted Triazines 13−15. We explored the replacement of terminal acetamide (**13**) with either a similar sulfonamide (**14**) or an inverted methylsulfonamide (**15**). Their synthesis is shown in Scheme 3.

Scheme 3. Synthesis of 2,4-Disubstituted Triazines 13−15

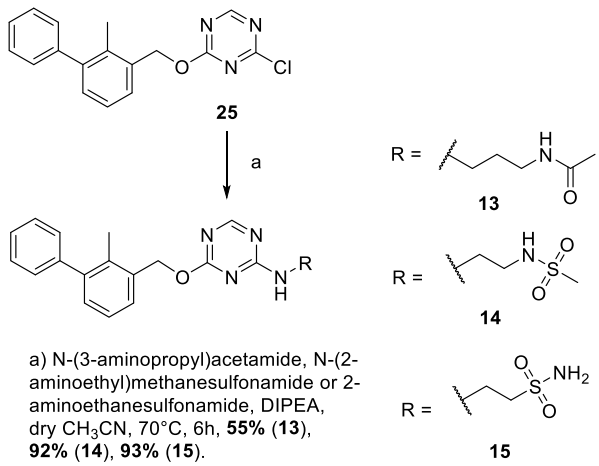

Starting from the earlier described chlorotriazine biphenyl ether **25**, nucleophilic substitutions were carried out employing *N*-(3-aminopropyl)acetamide (**13**), *N*-(2-aminoethyl)-methanesulfonamide (**14**), or 2-aminoethanesulfonamide (**15**) in the same reaction conditions reported previously (step **a**, Scheme 3; compare with step **b**, Scheme 2). Target 2,4-disubstituted triazines **13**−**15** were obtained in good to excellent yields.

https://doi.org/10.1021/acs.jmedchem.1c01409
J. Med. Chem. XXXX, XXX, XXX−XXX

Scheme 4. Synthesis of 2,4,6-Trisubstituted Triazines 16−18

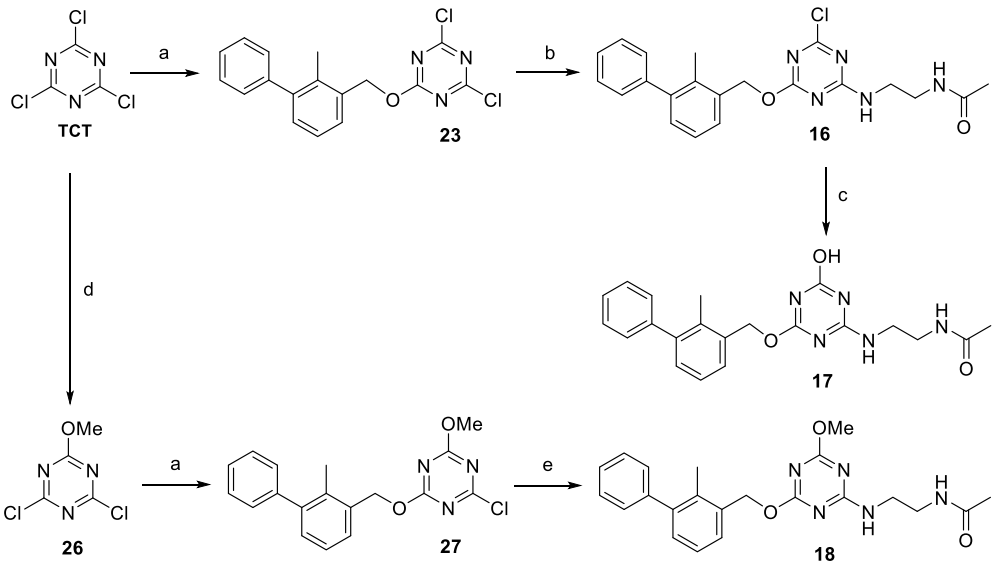

a) (2-methyl-[1,1'-biphenyl]-3-yl)methanol, DIPEA, dry DCM, -20°C or 0°C to rt, 2.5-4h, **70%** (**23**), **65%** (**27**); b) N-acetyl ethylenediamine, DIPEA, dry DCM, - 20° C to r.t., N_2 atm, 4h, **45%**; c) NaOAc, NMM, i-PrOH/H_2O 4:1, 0°C, then warmed to 50°C, 4 days, **30%**; d) $NaHCO_3$, dry MeOH, dry DCM, r.t., N_2 atm, 30min, **73%**; e) N-acetyl ethylenediamine, DIPEA, dry CH_3CN, 70°C, 5h, **69%**.

Scheme 5. Synthesis of Trisubstituted Methyl Triazine 19

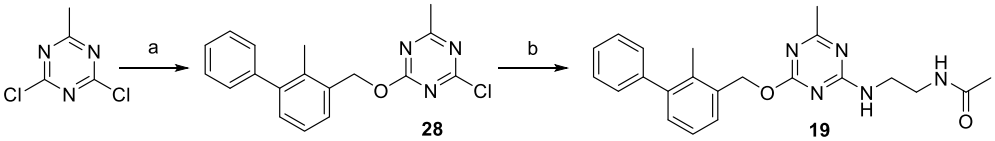

a) (2-methyl-[1,1'-biphenyl]-3-yl)methanol, DIPEA, dry CH_3CN, 40°C, N_2 atm, 24h, **22%**; b) N-acetyl ethylenediamine, DIPEA, dry CH_3CN, 60°C, N_2 atm, 24h, **48%**.

Exploration of Smaller Substituents on a Third Position: Synthesis of 2,4,6-Trisubstituted Triazines 16−19. In order to enlarge our preliminary SARs, we checked the compatibility of a third, small substituent with biological activity of triazine-based PD-L1 ligands. As first, we introduced small substituents with different chemical properties, such as a chlorine (**16**), hydroxy (**17**), and methoxy group (**18**) according to the strategy shown in Scheme 4.

2-Chloro-trisubstituted target **16** was obtained from earlier described dichloro biphenyl ether **23**, which underwent a nucleophilic substitution (step **b**, Scheme 4) with *N*-(2-aminoethyl)acetamide. Once more, the reaction temperature was initially set at −20 °C and gradually increased up to room temperature to avoid the risk of double substitution, due to the higher strength of an *N*-nucleophile. The reaction proceeded as expected, giving target 6-chlorosubstituted target **16** in moderate, unoptimized yields.

Target **16** was then reacted with water as a nucleophile to synthesize the hydroxy-substituted target **17** (step **c**). The reaction proceeded slowly, due to the poor nucleophilicity of water, and starting material **16** was still observed even after four days at 50 °C. The reaction was stopped to limit degradation of both starting **16** and target product **17**, and the latter was isolated in a poor, unoptimized 30% yield.

A similar strategy, using methanol as a nucleophile, was initially attempted to obtain target methoxy triazine **18**; unfortunately, even forcing reaction conditions, desired target **18** could not be obtained from chloro triazine **16**. Thus, we inverted the order of nucleophilic substitutions by introducing at first, the weaker O-nucleophile methanol in precedented, mild conditions (step **d**).[47] The reaction provided dichloromethoxy triazine **26** in good yields. A second nucleophilic substitution with (2-methyl-[1,1′-biphenyl]-3-yl)methanol was then performed in standard conditions, obtaining chloro diether intermediate **27** in good yields (step **a**). Finally, a third nucleophilic substitution with *N*-(2-aminoethyl)acetamide (step **e**, Scheme 4) was carried out in stronger reaction conditions and proceeded smoothly, affording 4-methoxy triazine target **18** in good yield.

The last trisubstituted synthetic target, methyl triazine **19**, was prepared from commercial dichloro methyl triazine, as depicted in Scheme 5.

2,4-Dichloro-6-methyl-1,3,5-triazine was submitted to a first nucleophilic substitution with (2-methyl-[1,1′-biphenyl]-3-yl)-methanol (step **a**, Scheme 5). Presuming a lower reactivity of methyl triazine in nucleophilic substitutions, such reaction was run at 40 °C for one day: notwithstanding residual starting material, the reaction was then stopped due to the appearance of multiple spots by thin-layer chromatography (TLC) monitoring. The desired methyl chlorobiphenylalkoxy triazine **28** was purified and isolated in low, unoptimized yields. Finally, intermediate **28** was submitted to a second substitution with

https://doi.org/10.1021/acs.jmedchem.1c01409
J. Med. Chem. XXXX, XXX, XXX−XXX

Table 1. Inhibitory Activity of Triazines 7−22 against PD-1/PD-L1 Interaction

General Structure

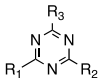

Compound	R_1	R_2	R_3	IC_{50} (μM)
7	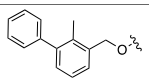	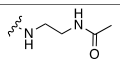	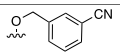	> 5
8	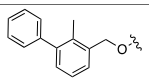	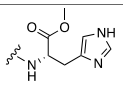	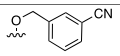	> 5
9	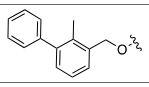	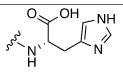	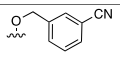	> 5
10	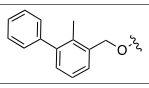	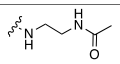		0.115 ± 0.024
11	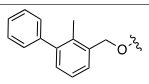	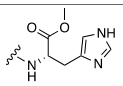		4.196 ± 0.680
12	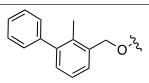	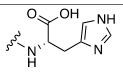		> 5
13	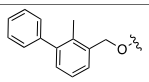	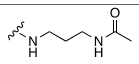		2.145 ± 0.519
14	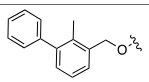	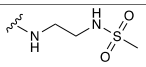		0.241 ± 0.058
15	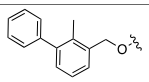	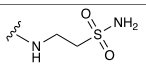		0.551 ± 0.133
16	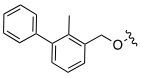	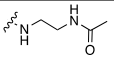		0.315 ± 0.016
17	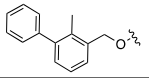	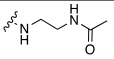		> 5
18	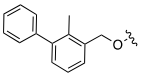	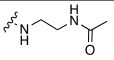		1.532 ± 0.075
19	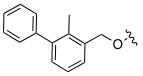	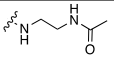		> 5
20	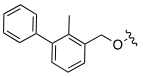	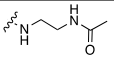	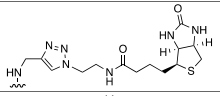	n.d.[a]
21	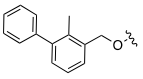	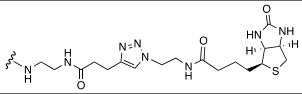		n.d.[a]
22	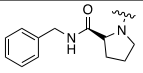	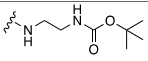		> 5
BMS-202				0.022 ±0.003

[a] IC_{50} determination was not possible due to the interference of the biotin moiety with the assay.

N-(2-aminoethyl)acetamide (step **b**, Scheme 5); hard reaction conditions were needed to drive the reaction to completion and obtain target 6-methyl-trisubstituted triazine **19** in moderate yields.

Synthesis of Triazines 20−22. Biotinylated derivatives were synthesized in order to confirm *in vitro* binding to PD-L1. Considering that a biphenyl ether moiety is important for PD-L1 binding,[33] we opted to introduce biotin either on the polar chain of a disubstituted triazine (**21**), as from modeling studies this moiety would point toward a solvent-exposed area not clashing with receptor surfaces, or biotin was introduced as a third substituent (R3 in Table 1) in a trisubstituted triazine (**20**). Short linkers were initially selected in order to connect functional groups suitable for click chemistry with our triazines, while limiting the molecular weight increase due to bioavailability concerns. Because both **20** and **21** showed efficacy in binding to cellular PD-L1, further efforts to study the linker/

https://doi.org/10.1021/acs.jmedchem.1c01409
J. Med. Chem. XXXX, XXX, XXX−XXX

Scheme 6. Synthesis of Biotinylated, Trisubstituted Triazine 20

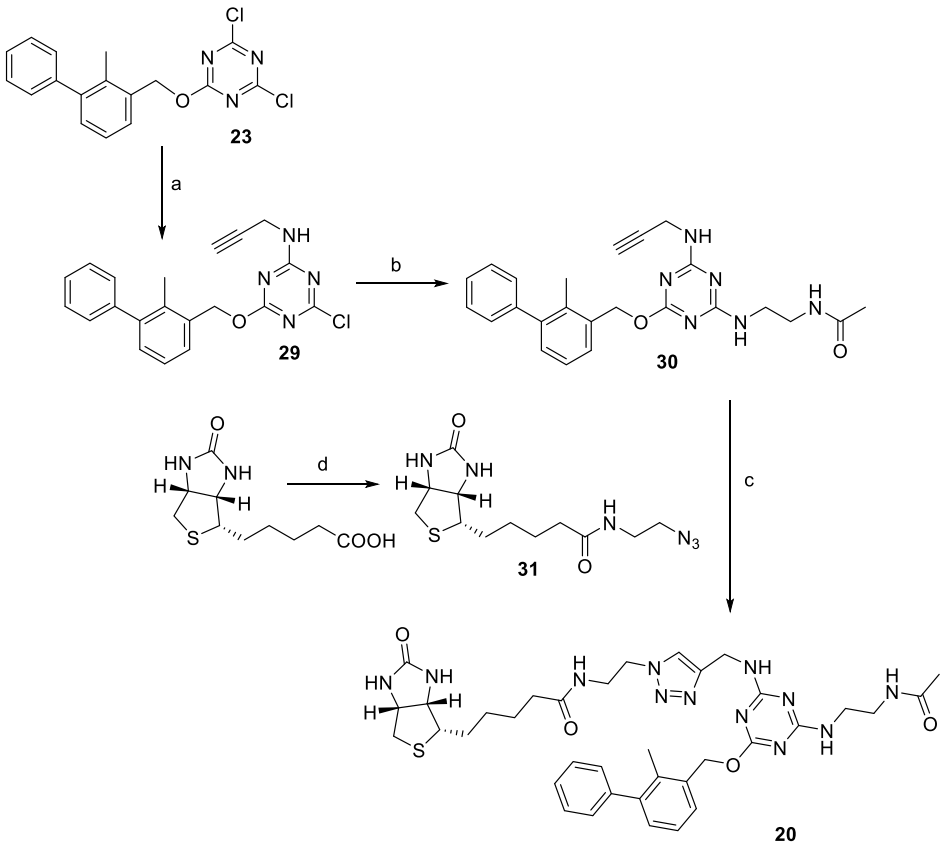

a) Propargylamine, DIPEA, DCM, -20°C to rt, 6h, **86%**; b) N-acetyl ethylenediamine, DIPEA, ACN, 60°C, 3h, **82%**; c) Na ascorbate, $CuSO_4 \cdot 5 \cdot H_2O$, THF/$H_2O$ 1:1, rt, 5h, **55%**; d) 2-azidoethylamine, HOBt, EDC, DIPEA, dry DMF, rt, 24 h, **74%**.

Scheme 7. Synthesis of Biotinylated, Disubstituted Derivative 21

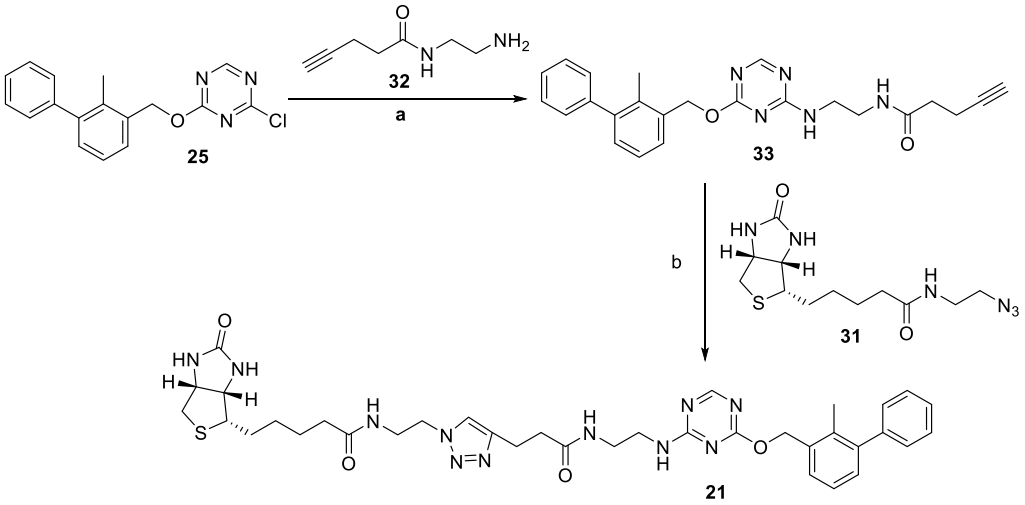

a) **32**, DIPEA, THF, 70°C, 8h, **46%**; b) Na ascorbate, $CuSO_4 \cdot 5 \cdot H_2O$, THF/$H_2O$ 1:1, rt, 5h, **49%**.

position influence were not carried out. The synthesis of biotinylated, trisubstituted triazine **20** is depicted in Scheme 6.

Dichloro biphenyl ether triazine **23** was reacted in mild nucleophilic conditions with propargylamine (step **a**, Scheme 6), obtaining chloroaminoalkynyl biphenyl ether triazine **29** in good yields. The latter was reacted with *N*-(2-aminoethyl)-acetamide (step **b**) in stronger conditions, affording alkynyl triazine **30** in good yields. Finally, a copper-catalyzed Huisgen 1,3-dipolar cycloaddition between alkenyl triazine **30** and azido biotinamide **31** in standard conditions (step **c**) yielded desired derivative **20** in moderate yields. Azido biotinamide **31** was prepared by simple amidation of biotin with commercial 2-azidoethylamine (step **d**, Scheme 6) in good yields.

https://doi.org/10.1021/acs.jmedchem.1c01409
J. Med. Chem. XXXX, XXX, XXX−XXX

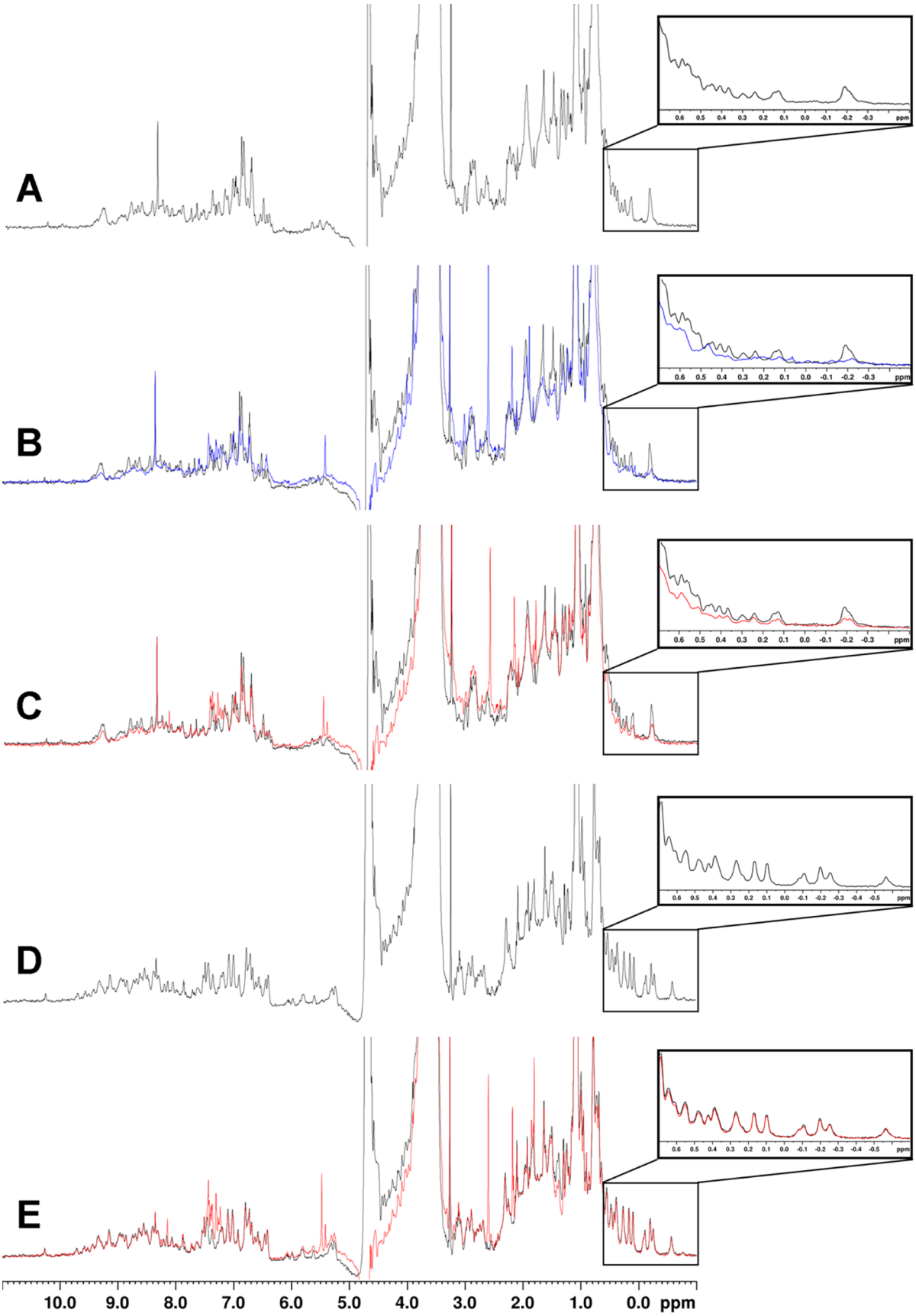

Figure 1. 1D-^{1}H NMR spectra of PD-L1 (10 μM, A, black) alone or in the presence of BMS-202 (**1**) (B, blue) and triazine **10** (C, red) and 1D-1H NMR spectra of PD-1 (10 μM, D, black) alone or in the presence of triazine **10** (E, red). The insets show the aliphatic regions used to monitor protein NMR signals in the absence and presence of the ligands.

https://doi.org/10.1021/acs.jmedchem.1c01409
J. Med. Chem. XXXX, XXX, XXX−XXX

The synthesis of biotinylated, disubstituted triazine **21** is shown in Scheme 7.

Previously described chloro biphenyl ether **25** underwent a nucleophilic substitution with known *N*-(2-aminoethyl)pent-4-ynamide **32**[48] (step **a**, Scheme 7), obtaining alkynyl triazine **33** in moderate yields. Target biotinylated, disubstituted triazine **21** was obtained in moderate yields through a Huisgen 1,3-dipolar cycloaddition between intermediate **33** with azido biotinamide **31** in standard conditions.

Finally, compound **22** (structure depicted in Table 1), lacking the pharmacophoric biphenyl moiety, was designed and synthetized as a congeneric negative control (see its synthesis in the Supporting Information).

NMR-Based Binding-Assay to Free PD-L1. 1D ^{1}H Macromolecule-based NMR experiments were used as a primary biophysical assay to detect the interaction between the free PD-L1 protein, expressed, and purified as previously described,[22,39] and all the newly compounds (**7**−**21**). Compound **22**, which was designed as a negative congeneric control, was also used for the NMR experiment. 1D ^{1}H NMR spectra of 10 μM PD-L1 were acquired in the presence of each ligand (1:1 and 1:10 protein/ligand ratios), and the NMR proton line width of the protein signals was analyzed to identify any putative ligand. Particularly, in such experiments, the chemical shift, as well as the reduction in intensity for the resonance signals of PD-L1, was monitored to follow the formation of a ligand−protein complex (Figures 1 and S1). We have compared the 1D ^{1}H NMR spectra of PD-L1 in the presence of the new investigated ligands with those of free PD-L1 and PD-L1 in the presence of the well-known binder BMS-202 (**1**), which has been exploited as a reference control. As an example, Figure 1 shows the comparison among the 1D ^{1}H NMR spectra of the free protein (Figure 1A), the protein in the presence of BMS-202 (**1**) (Figure 1B), and in the presence of our early lead **10** (Figure 1C). When **1** was added to PD-L1 at a stoichiometric ratio, a decrease in the intensity of the signals of the free protein, as well as the appearance of new signals, was observed (Figure 1B). Comparable results were obtained with triazine-based **10** (Figure 1C). In fact, the 1D ^{1}H NMR spectrum of PD-L1 in the presence of **10** is similar to that of PD-L1 induced by the presence of **1** in the line broadening of the signals for both protein−ligand complexes, which is much larger than that of the free protein (Figure 1A). This confirms unequivocally the formation of a **10**-PD-L1 complex, presumably with comparable features as the known **1**-PD-L1 complex. The formation of the complex between PD-L1 and the above-mentioned ligands is better highlighted through the comparison of the aliphatic regions of the spectra of the free protein (Figure 1A) with the two ligand−protein complexes (Figure 1B,C).

Similar results were obtained, for other compounds such as **13**−**16**, **18**, and **21** (Figure S1). For example, the 1D 1H NMR spectrum of PD-L1 in the presence of triazine **14** shows a reduction in the intensity for the proton signals of the protein comparable to that of PD-L1 induced by the presence of **1** or **10**. Differently, in the case of compound **22**, which was used as a negative reference compound, the absence of a reduction in the intensity of PD-L1 signals, even in the presence of high concentrations of the ligand, demonstrates that it does not interact with PD-L1 at all.

Finally, even if the compounds that turned out to be a PD-L1 binder at NMR experiments were designed for this receptor, further 1D 1H NMR experiments were carried out to probe a possible interaction even with PD-1, that was expressed and purified as previously described.[22,39] All the tested compounds resulted in not binding to PD-1. As an example, by comparing the 1D ^{1}H NMR spectra of PD-1 in the absence (Figure 1D) and in the presence of **10** (Figure 1E), the lack of any interaction is confirmed.

HTRF Assay. As a secondary, quantitative assay aimed to rank the novel, NMR-active triazine ligands based on their *in vitro* ability to inhibit the PD-1/PD-L1 interaction, a HTRF binding assay was used. This assay enables a simple and rapid characterization of inhibitors in a high-throughput format. Basically, it uses tagged human recombinant immune checkpoint partners (hPD1 and hPD-L1) and labeled antitag reagents for HTRF detection. More in detail, the interaction between hPD-L1 (Tag 1) and hPD1 (Tag2) is detected by using anti-Tag1 labeled with Europium (HTRF donor) and anti-Tag2 labeled with XL665 (HTRF acceptor). Upon hPD-L1 to hPD1 binding, the donor and acceptor antibodies are in close proximity, thus the excitation of the donor antibody triggers fluorescence resonance energy transfer (FRET) toward the acceptor antibody, which in turn emits specifically at 665 nm. Thus, compounds able to inhibit the PD1/PD-L1 interaction induce a reduction in the HTRF signal, which is directly proportional to the strength of the hPD1/hPD-L1 interaction.

Table 1 shows 16 triazine-based analogues, where variations in R_2 and/or R_3 established preliminary structure−activity relationships (SARs), which in turn help to better characterize the structural requirements to bind to PD-L1.

Among our newly synthesized triazines, disubstituted compound **10** displayed the highest inhibitory potency with an IC_{50} value of 115 (±24) nM. Therefore, this compound was selected for subsequent biophysical and biological evaluations, while molecular modeling studies were performed to rationalize results shown in Table 1.

Differential Scanning Calorimetry. Differential scanning calorimetry (DSC) experiments were carried out to compare the behavior of triazine **10** with that of standard pyridine BMS-202 **1** in binding and stabilizing the PD-L1 protein. If a compound binds preferentially to a folded protein, the melting temperature (T_m) of the latter will generally increase, and the tighter it binds, the more the Tm increases.[49] Therefore, we performed DSC experiments in which PD-L1 (32 μM) was heated in the absence and presence of both ligands (32 μM) to determine Tm variations. When no ligand was present, we observed a T_m value, corresponding to the maximum of the respective thermogram peak, of 46.5 (±0.5) °C. In the presence of either **10** or **1**, we observed T_m values of 49.0 (±0.5) °C and 53.0 (±0.5) °C, respectively. Hence, DSC analysis showed that both compounds significantly shifted the melting peak of PD-L1, indicating for both a direct binding with a change in the T_m of the protein (ΔT_m) of 2.5 and 6.5 °C for **10** and **1**, respectively (Figure S3). Subsequent molecular modeling helped to explain the different values recorded for the two compounds.

Molecular Modeling. In order to elucidate at an atomistic level, the binding mode of early lead **10** at the PD-L1 receptor, with the aim to rationalize both the HTRF and DSC results, molecular docking studies were performed. As for the protein tridimensional structure selection, the X-ray complex of homodimeric PD-L1 (monomers A and B) with the known inhibitor BMS-202 (**1**) (PDB code: 5J89) was chosen, based on the structural similarity between **1** and our triazine-based peptidomimetics. Docking of **10** predicted that it can be hosted, similarly to **1**, in the so-called cylindrical hydrophobic pocket defined at the interface between the two PD-L1 monomers.[40] In

https://doi.org/10.1021/acs.jmedchem.1c01409
J. Med. Chem. XXXX, XXX, XXX−XXX

detail, the 2-methylbiaryl moiety deepens in the bottom part of the binding site, engaging a T-shaped stacking interaction with the phenol moiety of $_{A}$Y56 as well as multiple lipophilic contacts with the side chains of $_{A}$M115, $_{B}$M115, and $_{B}$A121 (Figure 2),

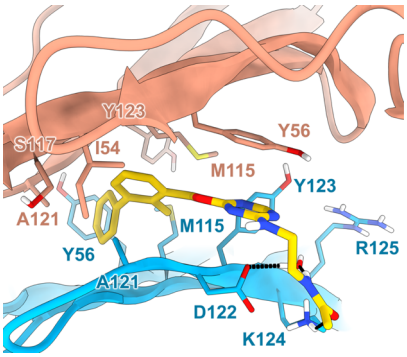

Figure 2. Docking-predicted binding pose of triazine **10** at the homodimeric PD-L1 binding site (PDB code: 5J89).[39] Protein monomers **A** and **B** are depicted as blue and red cartoons, respectively, while residues and water molecules important for ligand binding are highlighted as sticks. Ligand **10** is shown as yellow sticks, H-bonds are described as black dashed lines, and non-polar hydrogens are omitted for a better representation of the interactions.

analogously to what was earlier found for **1**. Besides, while the triazine core establishes a π-stacking with the $_{B}$Y56 side chain, the *N*-(2-aminoethyl)acetamide chain interacts through a water-bridge with the side chains of $_{A}$K124 and $_{A}$D122 and H-bonds with the cationic head of $_{A}$K124. Although the predicted binding mode of **10** is mostly superimposable with the crystallographic pose of **1** (Figure 3), important differences arise in the positioning of the central cores and in the interaction between the polar side chains and the receptor amino acids. The above-mentioned discrepancies are mostly due to the fact that the 1,3,5-triazine core, differently from the pyridine, provides a meta- and not a para-substitution, and thus spatially rearranges itself toward Y123 to properly orient the biphenyl moiety and the polar side chain along with the cylinder-shaped pocket (Figure 3). This observation would perfectly explain the marked loss of the binding of trisubstituted triazines **7**−**9** and can be ascribed to a steric clash between the third substituent on the triazine nucleus with the side chain of $_{A}$Y123 (Figure 3). Moreover, structural differences among the polar flexible chain of **10** and **1** seem to be further responsible for their different binding affinities. In fact, the aminoethyl group of **10** has a reduced basicity and a different distance from the triazine/pyrimidine with respect to that of **1**, thus affecting the interaction with the $_{A}$D22 side chain. Along the same line, our calculations suggest that the replacement of the *N*-(2-aminoethyl)-acetamide chain in compound **10** with bulky amino acids (such as histidine in **11** and **12**) poses problems of a simultaneous optimal accommodation of the biaryl moiety and the polar side chain. Accordingly, small changes in the ligand hydrophilic alkylamino chain (e.g., **13** and **14**) do not remarkably affect the overall ligand−receptor recognition process (Figure S4). Obviously, triazine **15**, where the inversion of the sulfonamide group with respect to **14** is present, cannot preserve the same water-mediated network of interaction with the residues $_{A}$D122 and $_{A}$K123, leading to a minor affinity for the PD-L1 ligand.

Cytotoxicity of 10 in Normal and Cancer Cells Expressing Different Levels of PD-L1. In order to determine the PD-1/PD-L1-dependent cytotoxicity of disubstituted triazine **10**, we first measured the expression levels of PD-L1 in both cancer and non-cancer cells. As shown in Figure 4, human peripheral blood mononuclear cells (PBMCs) almost did not express PD-L1, while immortalized human keratinocytes (HaCaT) and pulmonary adenocarcinoma cells (PC9) showed a moderate PD-L1 expression. Conversely, high PD-L1 levels were detected in lung adenocarcinoma cells (HCC827). Noteworthily, treatment with IFNγ significantly ($P < 0.001$) upregulated the expression of PD-L1 in both PC9 and HCC827 cells, with a higher ($P < 0.05$) expression in HCC827 cells. We next investigated the growth inhibitory effects of **10** in both normal and cancer cells expressing different levels of PD-L1 (Figure 4). PBMCs, HaCaT, PC9, and HCC827 cells were treated with a range of concentrations (0.1, 1, 10, or 100 μM) of pyridine-based **1** as a known, positive control, and our disubstituted triazine **10**. Following 24 and 48 h of incubation times, no significant cytotoxicity was observed for both **1** and **10** at 10 μM. A cytotoxic effect for both **1** and **10** was detected either in normal and cancer cells when applied at 100 μM, regardless of the PD-L1 expression levels. However, pyridine-based **1** ($P < 0.05$) inhibited cell growth in general, and in PBMCs in particular, significantly more than our triazine-based **10** (Figure 5). Moreover, compound **10** did not affect PBMC proliferation following 24 h of incubation.

Co-Localization of PD-L1 with Biotinylated Derivatives of 10. In order to confirm the binding of **10** to membrane-embedded PD-L1, we performed an immunofluorescent double-staining to study the possible interaction between the cell surface PD-L1 and earlier described biotinylated triazine derivatives **20** and **21** on PBMCs, PC9, and HCC827 cells. As

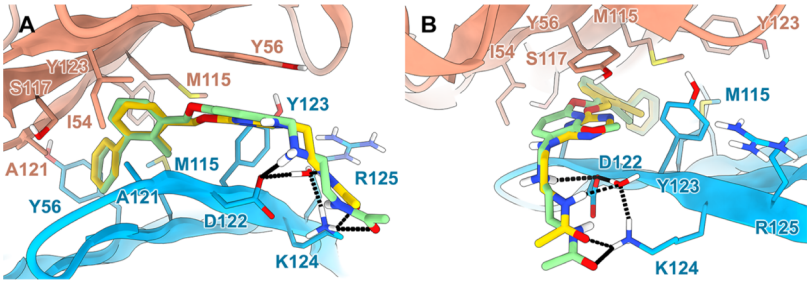

Figure 3. Side view (A) and bottom view (B) of the superposition between the docking-predicted binding pose of triazine **10** (gold sticks) and the X-ray structure of pyridine **1** (green sticks) at the homodimeric PD-L1 binding site (PDB code: 5J89).[39] Protein monomers **A** and **B** are depicted as blue and red cartoons, respectively; important residues for ligand binding are shown as sticks. H-bonds and π-stacking are indicated with black dashed lines, non-polar hydrogens are omitted for a better representation of the interactions.

https://doi.org/10.1021/acs.jmedchem.1c01409
J. Med. Chem. XXXX, XXX, XXX−XXX

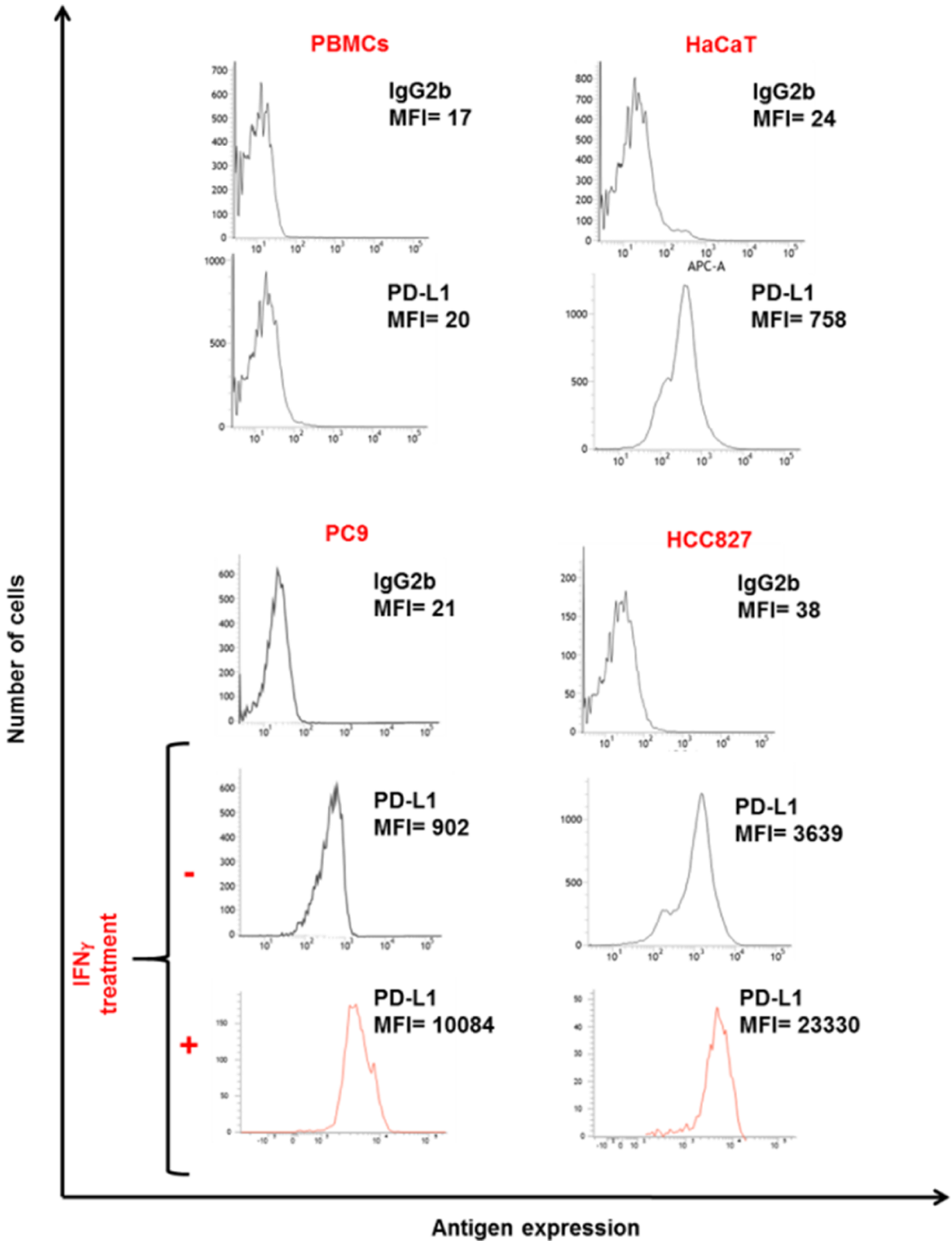

Figure 4. PD-L1 expression levels in normal and cancer cells. PBMCs, HaCaT, PC9, and HCC827 cells were seeded at a density of 2×10^5 per well in 6-well plates and incubated with IFNγ (100 IU/mL). Untreated cells were used as a control. Following 24 h of incubation at 37 °C in a 5% CO_2 atmosphere, cells were harvested, and the cell surface was stained with an allophycocyanin (APC)-conjugated PD-L1-specific mouse monoclonal antibody (clone 29E.2A3). APC-conjugated mouse IgG2b was used as a specificity control. Representative results are shown.

shown in Figure 6, the PD-L1 expression co-localizes with both **20** and **21** in PC9 and HCC827 cells, which expressed different levels of PD-L1. In contrast, as expected, biotinylated **20** and **21** were not detected in PBMCs, which do not express PD-L1.

***In Vitro* Immunomodulatory Activity of 10.** To assess the immunomodulatory activity and the putative functional significance of PD-L1 inhibition by **10**, the effect of stimulated PBMCs on the recognition and destruction of cancer cells,

https://doi.org/10.1021/acs.jmedchem.1c01409
J. Med. Chem. XXXX, XXX, XXX−XXX

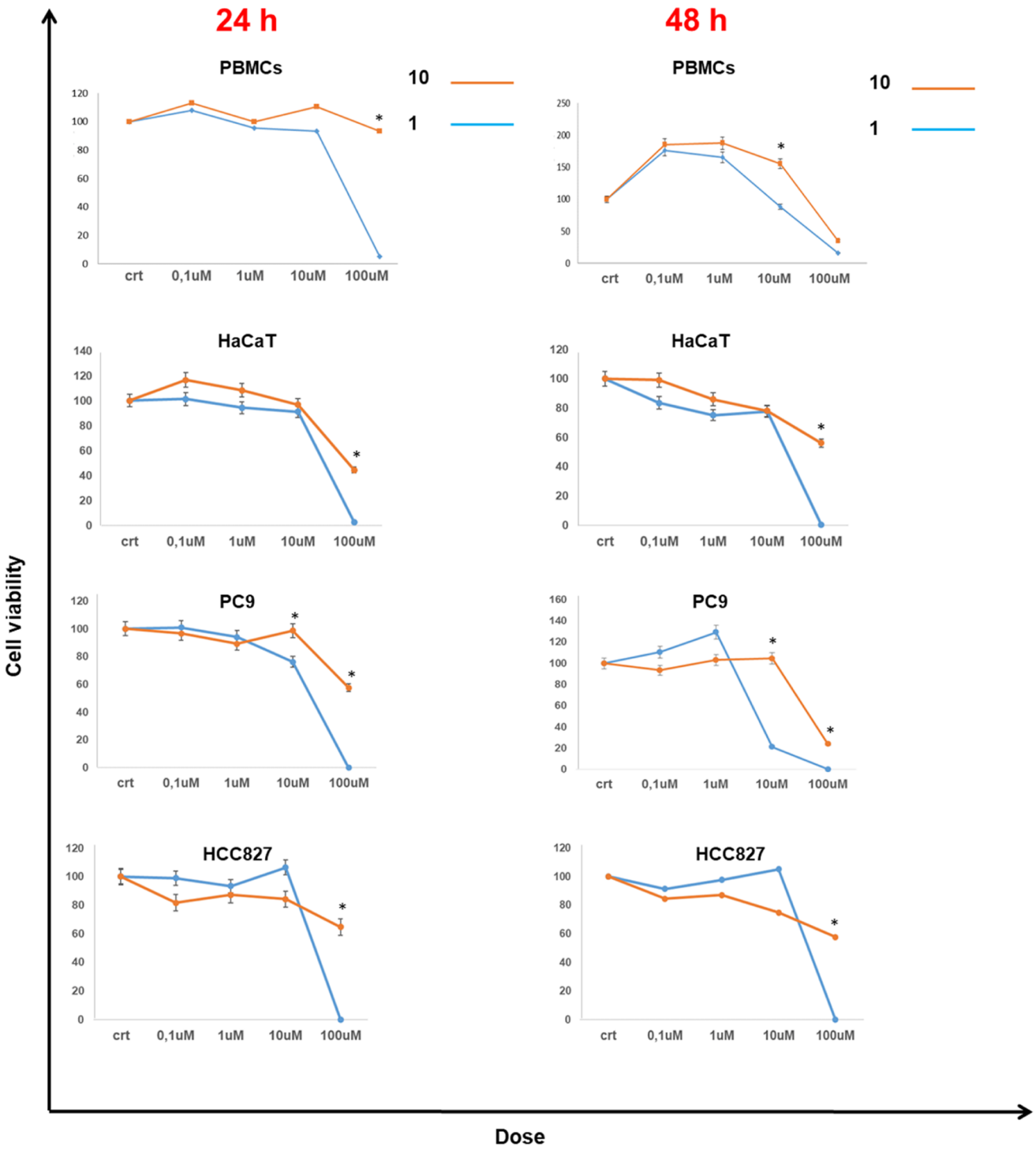

Figure 5. Effects of 10 and 1 on cell viability of normal and cancer cells expressing different levels of PD-L1. PBMCs, HaCaT, PC9, and HCC827 cells were seeded in triplicate in 96-well microtiter plates at a density of 1×10^4 per well and incubated with the indicated doses of triazine **10** or pyridine standard **1**, the latter used as a control for PD-L1 inhibition. Untreated cells were used as a control. DMSO (vehicle for both **10** and **1**) concentration was maintained at 0.02% in all wells. Following 24 and 48 h of incubation, at 37 °C in a 5% CO_2 atmosphere, cell viability was determined by a cell counting kit-8 (CCK-8) assay. Data are expressed as a mean percent of survival rate ± SD of treated cells as compared to the untreated cells. A mean percent of the survival rate and SD was calculated from three independent experiments performed in triplicate. The difference between cytotoxic doses of **10** and **1** was calculated using an unpaired *t*-test. * indicates $P < 0.001$.

f7

following treatment with **10**, was investigated and compared to that induced by **1** as a control. As shown in Figure 7, stimulated PBMCs recognized both PC9 and HCC827 cells because co-culturing of stimulated PBMCs and cancer cells significantly induced morphological changes of both PC9 and HCC827 cells (Figure S5) and increased IFNγ release ($P < 0.001$) as compared to non-stimulated PBMCs. Specifically, typical signs of cellular damage, including pleomorphism, rupture of the nuclear or plasma membrane, nuclear fragmentation, a shrunken cytosol, and disruption of the intercellular junctional complexes, were

https://doi.org/10.1021/acs.jmedchem.1c01409
J. Med. Chem. XXXX, XXX, XXX−XXX

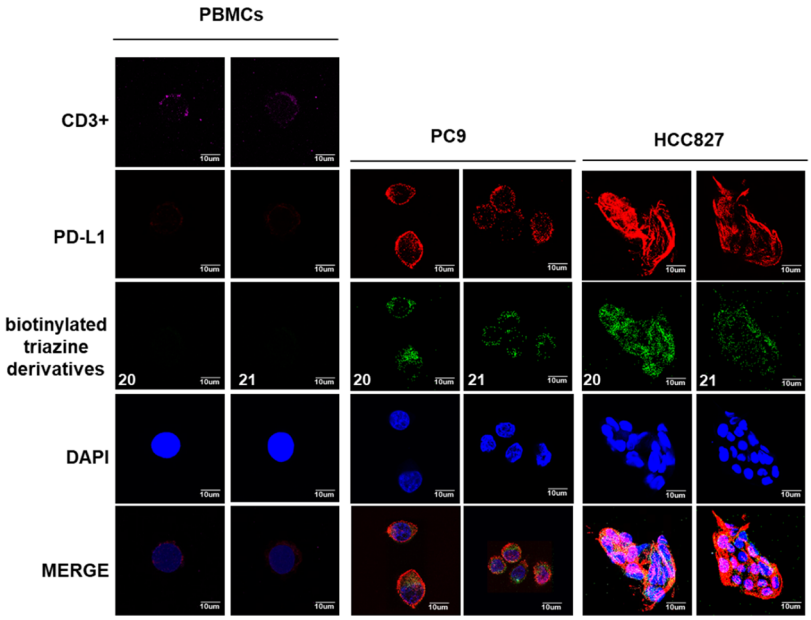

Figure 6. Co-localization of biotinylated triazines **20**, **21**, and PD-L1 in the normal and cancer cells expressing different levels of PD-L1. PBMCs, PC9, and HCC827 cells were incubated with biotinylated derivatives **20** and **21** at 1 μM. Following 8 h of incubation, cells were stained with PD-L1-specific (Ab 205921) and a CD3-specific monoclonal antibodies (Ab17143). Biotinylated **20** and **21** were detected utilizing a streptavidin-FITC-conjugated antibody (*green*). PD-L1 and CD3 expressions were detected utilizing Alexa Fluor-555 (*red*)- and Alexa Fluor-649 (*violet*)-conjugated anti-rabbit IgG and anti-mouse IgG1. Nuclei were stained by 4′,6-diamidino-2-phenylindole (DAPI) (*blue*). Representative immunofluorescent staining is shown. Scale bars are indicated.

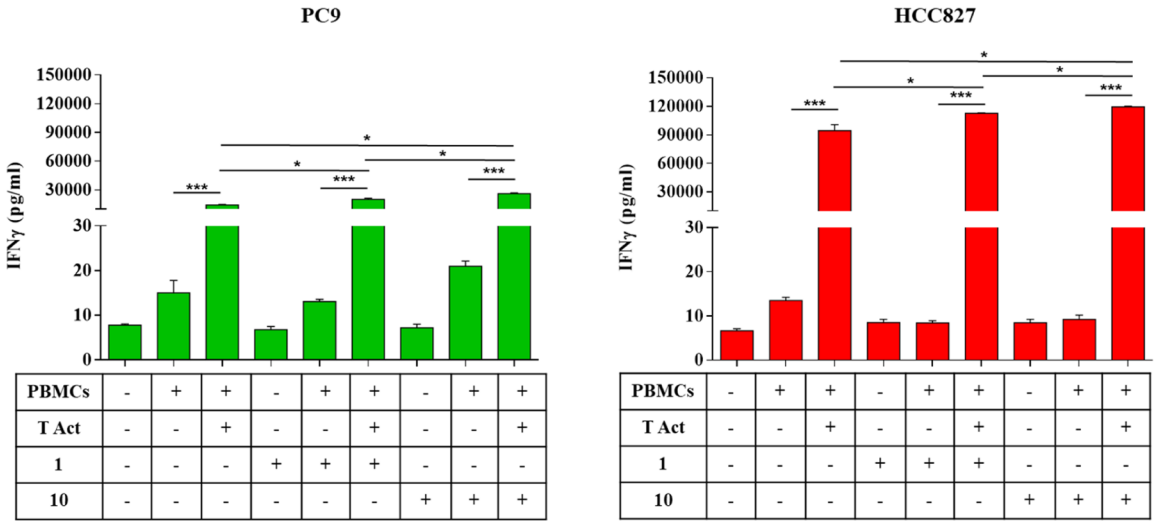

Figure 7. Enhancement of IFNγ release by stimulated PBMCs co-cultured with PD-L1 expressing cancer cells in the presence of triazine **10**. PC9 (green) and HCC827 cells (red) were co-cultured with stimulated PBMCs and treated with either triazine **10** (1 μM) or pyridine compound **1** (1 μM). Compound 1 was utilized as a control for triazine 10. PBMCs were stimulated utilizing an anti-CD3 (1 μg/mL) and an anti-CD28 (1 μg/mL) T Cell TransAct (T Act). Non-stimulated PBMCs and untreated cancer cells were used as controls. Following 48 h of incubation, IFNγ levels in the medium harvested from cultures of PBMCs with cancer cells were measured by an ELISA Max Deluxe Set Human IFNγ kit. Data are expressed as IFNγ levels ± SD of the results obtained in three independent experiments; each of them performed in triplicate. *Indicates $P < 0.01$. *** Indicates $P < 0.001$. All the P values were calculated using the two-sided student's *t*-test.

observed. Noteworthily, these morphological changes were significantly increased when the PC9 and HCC827 cells were previously incubated either with **10** or **1** (1 μM). The morphological changes induced by treatment with **10** and **1** in cells co-cultured with stimulated PMBCs were higher in HCC827 than in PC9 cells. Conversely, no significant changes on cancer cells were detected by either non-stimulated co-cultured PBMCs, by treatment with **10** or **1**, a single agent or in combination, in the absence of PBMCs. Moreover, treatment with both **10** and **1** significantly ($P < 0.01$) increased IFNγ release by co-cultured stimulated PBMCs as compared to untreated and treated cells as well as to co-cultured stimulated PBMCs without treatment with **10** or **1** (Figure 7). Again, IFNγ release induced by treatment with **10** and **1** in cells co-cultured with stimulated PMBCs was higher in HCC827 than in PC9cells. Lastly, treatment with **10** or **1** significantly ($P < 0.01$) inhibited survival (Figure 8) and increased apoptotic induction (Figure 9) for PC9 and even more in a greater extent

https://doi.org/10.1021/acs.jmedchem.1c01409
J. Med. Chem. XXXX, XXX, XXX−XXX

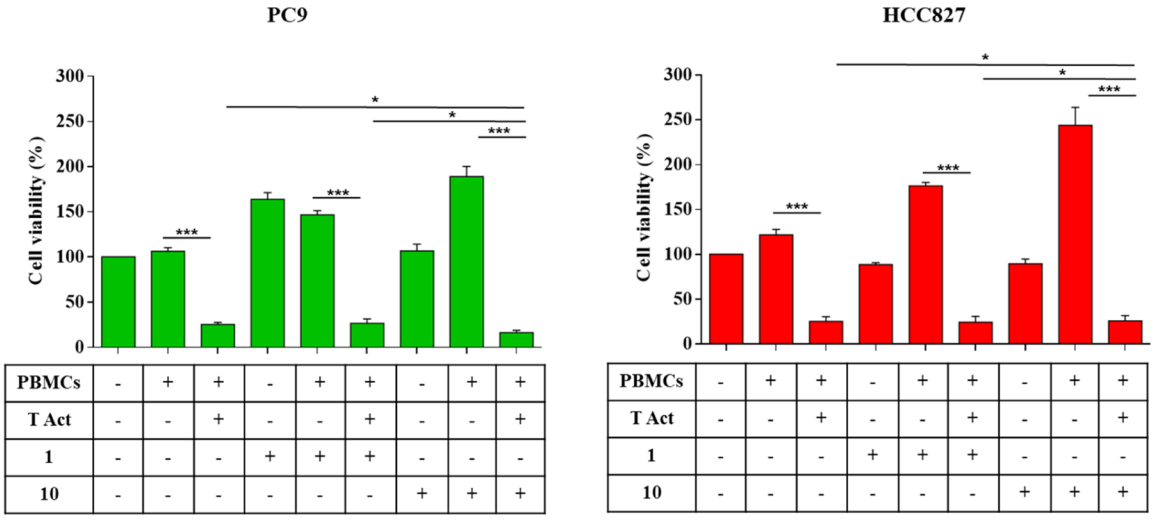

Figure 8. Reduction of cell viability of PD-L1 expressing cancer cells co-cultured with stimulated PBMCs in the presence of triazine **10**. PC9 (green) and HCC827 cells (red) were co-cultured with stimulated PBMCs and treated with either triazine **10** (1 μM) or pyridine compound **1** (1 μM). Compound 1 was utilized as a control for triazine **10**. PBMCs were stimulated utilizing an anti-CD3 (1 μg/mL) and an anti-CD28 (1 μg/mL) T Cell TransAct (T Act). Non-stimulated PBMCs and untreated cancer cells were used as controls. Following 48 h of incubation, cell viability was determined by cell counting kit-8 (CCK-8) assay. Cancer cells from the cultures of PBMCs were isolated by removing PBMCs with phosphate-buffered saline (PBS) washing. Data are expressed as a mean percent of survival rate ± SD of the treated cells as compared to untreated cells. The mean percent of the survival rate and SD were calculated from three independent experiments performed in triplicate. *Indicates $P < 0.05$. *** Indicates $P < 0.001$. All the P values were calculated using the two-sided Student's *t*-test.

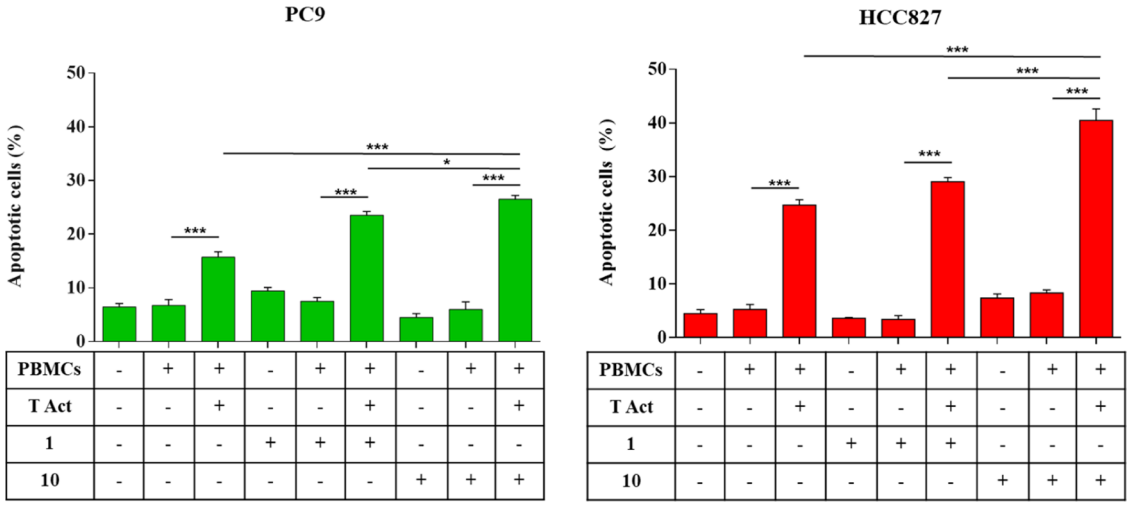

Figure 9. Enhancement of apoptosis induction of PD-L1 expressing cancer cells co-cultured with stimulated PBMCs in the presence of triazine **10**. PC9 (green) and HCC827 cells (red) were co-cultured with stimulated PBMCs and treated with either triazine **10** (1 μM) or pyridine standard **1** (1 μM). Compound **1** was utilized as a control for triazine **10**. PBMCs were stimulated utilizing an anti-CD3 (1 μg/mL) and an anti-CD28 (1 μg/mL) T-cell TransAct (T Act). Non-stimulated PBMCs and untreated cancer cells were used as controls. Following 48 h of incubation, apoptosis induction was determined by flow cytometry analysis of annexin V and propidium iodide (PI) staining. The levels of apoptosis are plotted and expressed as a mean fraction of annexin V^+ cells ± SD of the results obtained in three independent experiments. *Indicates $P < 0.05$. *** Indicates $P < 0.001$. All the P values were calculated using the two-sided Student's *t*-test.

for HCC827 cells by co-cultured stimulated PBMCs as compared to untreated and treated cells as well as to co-cultured stimulated PBMCs without treatment with **10** or **1**. Interestingly, triazine-based **10** increased IFNγ release, inhibited survival, and increased apoptotic induction in PC9 and HCC827 cells in a significantly ($P < 0.05$) greater extent as compared to cells incubated with pyridine compound **1**.

Exosome Purification and NMR-Based Binding Assay of 10. Increasing evidence indicates that exosomes derived from cancer cells can regulate the TME promoting cancer progression via their cargos, which mainly include proteins, lipids, and nucleic acids.[50,51]

To this regard, recent studies have demonstrated that PD-L1 is expressed even on the surface of exosomes (ExoPD-L1) and that its level mostly reflects the PD-L1 level of their parental cells.[2] ExoPD-L1 efficiently binds PD-1 on the surface of lymphocytes both in tumor foci and far from the cancer site,[2] and thus, distant tumor cells can remotely attack activated T cells by ExoPDL1 and this strategy, at least in the long run, seems much more effective than the release of soluble PD-L1, which would be easily degraded by proteolytic enzymes. Last but

https://doi.org/10.1021/acs.jmedchem.1c01409
J. Med. Chem. XXXX, XXX, XXX−XXX

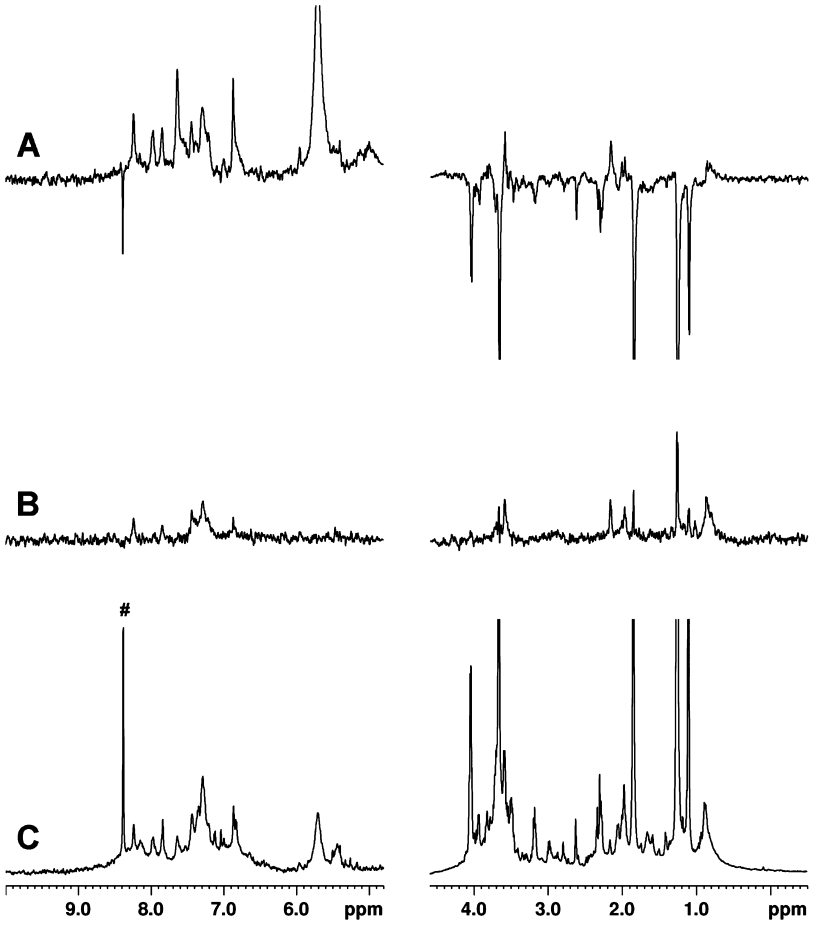

Figure 10. 1D-1H NMR spectrum (C), STD spectrum (B), and WL spectrum (A) of compound **11** (0.5 mM) in the presence of ExoPD-L1. The impurity is marked with a hash symbol.

not least, exosomes were recently demonstrated to even be able to transport PD-L1 from PD-L1-positive to PD-L1-negative cancer cells, thus playing a key role in immunosuppression.[52] Hence, it is of outmost importance to develop molecular entities able to hamper both ExoPD-L1 as well as cellular PD-L1. Accordingly, we decided to challenge compound **11** in binding with ExoPD-L1. First, according to the literature, we selected three cell lines expressing a high level of PD-L1 exosomes: two human NSCLC lines (A549 and H460) and one breast cancer cell line (BT459).[53] The detection of PD-L1 on exosomes was confirmed through an ELISA assay (see the Methods section for details and Supporting Information for Figure S6). Then, saturation transfer difference NMR (STD-NMR)[54] and Water-Logsy-NMR (WL-NMR)[55] experiments were acquired using exosomes and compound **11**. Both experiments focus on the NMR signals of the ligand and use the magnetization transfer by the nuclear overhauser effect (NOE) between the protein and ligand. If binding is very tight, the magnetization transfer to ligand molecules is not very efficient,[56] thus, compound **11**, a close analogue of **10**, but endowed with a higher IC_{50} was chosen. The presence of signals in STD-NMR (Figure 10B), and positive peaks in WL-NMR (Figure 10A) experiments, strongly indicate an interaction between the ligand and PD-L1 protein on exosomes.

In Silico Physicochemical Properties' Prediction for Compounds 1, 5, and 10. An *in silico* prediction of the physicochemical properties of our compound **10** has been performed using Qikprop software (Schrödinger, LLC New York). The out coming profile was compared with those of BMS-202 (**1**) and compound **5**, both calculated with Qikprop software. To analyze the results, we considered ideal ranges as indicated by Qikprop itself, the Lipinski's rule of five, the rule of three, and linear regression approach for the prediction of blood−brain barrier (BBB) permeability. As shown in Table S1, compound **10** exhibits fully suitable physicochemical properties with no detected violations, and all our measurements suggest that its properties should determine an acceptable pharmacokinetic profile and favor passive diffusion across the BBB. Differently, **5** displays two violations of the rule of five, two of the rule of three, and some parameter values not ideal for the BBB penetration, while **1** does not display any violation but, as well as **5**, two parameters' values are not ideal for BBB permeability.

■ CONCLUSIONS

Inhibition of the PD-1/PD-L1 axis by monoclonal antibodies has achieved remarkable success in treating a growing number of cancers. However, the recent discovery of BMS-202 (**1**) has fueled efforts directed to a novel class of small molecules as direct and potent PD-L1 inhibitors. In this respect, the development of structurally new PD-L1 small ligands would be of utmost importance for a complete understanding of the full theranostic potential of small-molecule PD-L1/PD-1 inhibitors. Herein, a series of 2,4,6-tri- and 2,4-disubstituted 1,3,5-triazines was synthesized and assayed for their PD-L1 binding first by NMR and then through HTRF assays. Disubstituted triazine **10** endowed with a nanomolar IC_{50} was also subjected to DSC

https://doi.org/10.1021/acs.jmedchem.1c01409
J. Med. Chem. XXXX, XXX, XXX−XXX

experiments to compare its behavior with positive standard **1** in binding and stabilizing the PD-L1 protein. Furthermore, through NMR, **10** was shown to specifically bind to PD-L1 and not to PD-1. Then, to demonstrate that triazine **10** binds not only to isolated PD-L1 but also when embedded into cell membranes, we used two biotinylated triazine derivatives (**20** and **21**) in an immunofluorescent double-staining assay on PBMCs, PC9, and HCC827 cells. Early lead **10** was demonstrated to bind PD-L1 on cell membranes, thus restoring the function of PBMCs co-cultured with lung adenocarcinoma PC9 and HCC827 cells. Indeed, an increased IFN-γ secretion and an augmented apoptotic induction on PC9 and HCC827 cancer cells were clearly visible upon treatment with both **10** or **1**. Interestingly, even if in HTRF and in DSC assays standard triazine **1** showed a stronger PD-L1 binding with respect to **10** (22 *vs* 115 nM IC_{50s}, respectively), in cell assays, triazine **10** was slightly (PC9 cells) or significantly more (HCC827) active than **1** in inducing apoptosis after PBMC reactivation. Moreover, **10** demonstrated a lower cytotoxicity in healthy cells (lower off-target effect) and a higher induction of IFN-γ in treated cancer cells than standard **1**.

Today, in a fast-growing field, the identification and characterization of structurally new, direct PD-L1 binders is of utmost importance to largely unravel the full potential of this brand-new class of small-molecule immunomodulatory leads. With this in mind, and on the basis of the herein presented encouraging data, further development for triazine-containing inhibitors is expected. Noteworthily, the structural insights into the binding mode of **10** on the PD-L1 surface, together with a comparison with the binding mode for **1** surely, add another piece to the precious puzzle of PD-L1/small-molecule interactions. Finally, due to the recent discoveries of the importance of ExoPD-L1 as both a tumor and metastasis promoter and as a possible non-invasive biomarker to predict immunotherapeutic response, the capability of a close analogue of **10** (with a lower IC_{50} most suitable for STD experiments) to bind ExoPD-L1 was challenged. The propensity of our molecule to directly bind the ExoPD-L1, which has never been demonstrated for small PD-L1 ligands so far, opens up a new perspective for this series of molecules in a wider range of preclinical or diagnostic applications.

■ EXPERIMENTAL SECTION

Protein Expression and Purification. The proteins were expressed and purified as described by Holak et al.,[22,39] implementing the extraction method through multiple cycles of sonication and buffers.

The plasmid encoding an hPD-L1 (amino acids 18−134) construct and the plasmid encoding an hPD-1 (amino acids 33−150) construct were cloned into two different pET-21b(+) and expressed in *Escherichia coli* BL21(DE3) gold strain cells. The protocols for the expression and purification of the proteins are the same for hPD-L1 and PD-L1. pET-21b(+)-transformed cells were cultured in LB medium supplied with ampicillin (0.1 mg mL^{-1}). A drop of antifoam was then added, and the culture was shaken at 37 °C until OD reached 0.60. Protein overexpression was induced with 1 mM IPTG, and the culture further shaken at 37 °C for 16 h. Cells were harvested by centrifugation. The supernatant was discarded, whereas the pellet was resuspended in 20 mM Tris−HCl, pH 8.0 buffer (40 mL per liter of culture). Because the protein was expressed as inclusion bodies, it was extracted by several cycles in denaturing conditions, and then refolded. In particular, after homogenization, the suspension containing the inclusion bodies was sonicated for 10 cycles, alternating 30 s of sonication and 3 min of resting, and then ultracentrifuged. The supernatant (soluble fraction) was discarded, whereas the pellet was resuspended in 50 mM Tris−HCl, pH 8.0, 200 mM NaCl buffer (40 mL per liter of culture), supplemented with 10 mM ethylenediaminetetraacetate and 10 mM 2-mercaptoethanol (BME). The mixture was again homogenized, and then sonicated for five cycles. The suspension was ultracentrifuged, then the supernatant (washing fraction) was discarded, whereas the pellet was redissolved in 50 mM Tris−HCl, pH 8.0, 200 mM NaCl, 6 M GdmCl buffer (20 mL per liter of cultures) supplemented with 10 mM BME. The mixture was homogenized, then sonicated for 5 cycles, and finally ultracentrifuged. The residual pellet was discarded, whereas the supernatant (GdmCl stock) was stored at 4 °C. The GdmCl stock containing unfolded hPD-L1 was slowly diluted 15 times in 100 mM Tris−HCl, pH 8.0, 1 M L-arginine solution supplied with 0.25 mM oxidized glutathione and 0.25 mM reduced glutathione, under vigorous magnetic stirring. The solution of the refolded protein was incubated at 4 °C under magnetic stirring for 6 h, and then extensively dialyzed against 50 mM Tris−HCl, pH 8.0, 150 mM NaCl buffer. The protein solution was taken out from dialysis, and then filtered with a 0.20 μm filter. The solution was concentrated and purified by size exclusion chromatography on a Hi-Load 26/60 Superdex 75pg column (GE Healthcare), previously equilibrated with 10 mM Tris−HCl, pH 8.0, 20 mM NaCl buffer. Elution was performed at 2.5 mL/min and fractions containing hPD-L1 were identified by Coomassie staining SDS-PAGE and collected. The solution of pure protein was supplied with 0.1% NaN_3 and protease inhibitors (Roche), and then stored at 4 °C for NMR experiments. The protein folding was evaluated by NMR.

NMR Sample Preparation. 600 μL of 10 μM hPD-L1 and hPD-1 in 10 mM Tris−HCl, pH 8.0, 20 mM NaCl buffer, and 10% D_2O were prepared for 1D ^{1}H NMR free hPD-L1 and hPD-1 assays.

BMS-202 **1** [10 and 100 μM solutions, previously solubilized in dimethyl sulfoxide-d6 (DMSO-d_6)] were added to 600 μL of 10 μM hPD-L1 in 10 mM Tris−HCl, pH 8.0, 20 mM NaCl buffer, and 10% D_2O for the 1D ^{1}H NMR control evaluation of the hPD-L1—BMS-202 interaction.

In the 1D ^{1}H macromolecule-based NMR screening experiments with our triazine library, each sample was similarly prepared. 10 and 100 μM of each ligand (previously solubilized in DMSO-d_6) were added to 600 μL of 10 μM hPD-L1 in 10 mM Tris−HCl, pH 8.0, 20 mM NaCl buffer, and 10% D_2O. For each analysis, the samples were then transferred to a 5 mm NMR tube.

Early lead triazine **10** [10 and 100 μM solutions, previously solubilized in dimethyl sulfoxide-d6 (DMSO-d_6)] were added to 600 μL of 10 μM of hPD-1 in 10 mM Tris−HCl, pH 8.0, 20 mM NaCl buffer, and 10% D_2O for the 1D ^{1}H NMR evaluation of the hPD-L1—**10** interaction.

In the 1D 1H ligand-based NMR STD and WL experiments, 0.5 mM of compound **11** (previously solubilized in DMSO-d_6) were added to 200 μL of ExoPD-L1 containing 10% of deuterium oxide and then transferred to a 3 mm NMR tube.

NMR Spectroscopy. For the 1D ^{1}H macromolecule-based NMR screening, all experiments were acquired on a Bruker AVANCE NEO NMR spectrometer operating at 700 MHz (^{1}H Larmor frequency), equipped with a 5 mm TCI 3 channels HCN cryo-probehead and a room-temperature probe head, optimized for ^{1}H sensitivity. The spectrometer was also equipped with SampleCase (autosampler) for NMR screening.

All spectra were acquired at 298 K, using 256 scans per spectrum with a recovery delay of 1.5 s. The spectra were calibrated with respect to the water frequency; the H_2O signal was suppressed using excitation sculpting with gradients[57] and NMR spectra were phase adjusted and baseline corrected. The spectra were processed and analyzed with the Bruker TOPSPIN 4.0.7 software package.

1D ^{1}H spectra of hPD-L1 were recorded prior and after the addition of each triazine compound in a 1:1 M ratio with respect to the protein. A ligand excess (10-fold higher with respect to the protein) was also tested to detect weaker interactions. This method relies on monitoring the chemical shift and line broadening changes of the signals of a protein in the aliphatic and aromatic regions, upon the protein interaction with a small molecule.

For the 1D ^{1}H ligand-based NMR, all experiments were acquired on a Bruker AVANCE NEO NMR spectrometer, operating at 600 MHz

https://doi.org/10.1021/acs.jmedchem.1c01409
J. Med. Chem. XXXX, XXX, XXX−XXX

(^{1}H Larmor frequency), equipped with a 5 mm QCI H-P/C/N-D-5-Z CryoProbe, and optimized for ^{1}H sensitivity. The spectrometer was also equipped with SampleJet (autosampler).

STD-NMR spectra were acquired with 512 scans, 2.0 s of saturation time, and 40 ms of spin-lock with on-resonance irradiation at −1.0 for the selective saturation of protein resonances and off-resonance irradiation at −200 ppm for reference spectra. STD-NMR spectra were obtained by the internal subtraction of the saturated spectrum from the reference spectrum by phase cycling with a spectral width of 19 ppm, relaxation delay of 3 s, 32 k data points for acquisition, and 64 k for transformation. STD effect is calculated as the signal to noise. WL NMR experiments were acquired with 512 scans, 1.7 s of saturation time, and 40 ms of spin lock for the selective saturation of protein resonances.

HTRF Assay. Inhibition of the PD-1/PD-L1 interaction was tested using the PD-1/PD-L1 HTRF binding assay kit from Cisbio (US). The experiments were performed according to the manufacturer's guidelines (https://www.cisbio.com/usa/drug-discovery/human-pd1pd-l1-biochemical-interaction-assay). The IC_{50} values for PD-1/PD-L1 inhibition were determined by analyzing the log of the concentration versus response curves using the Origin Software version 7.0.

DSC. DSC measurements were carried out using a Nano-DSC (TA Instruments, New Castle, DE, USA). The experiments were performed at a 32 μM PD-L1 concentration in 10 mM Tris−HCl buffer at pH 8.0, with 20 mM NaCl, in the absence and presence of pyridine standard **1** or triazine **10** (32 μM). Scans were performed at 0.5 °C/min in a 10−100 °C temperature range. A buffer−buffer scan, under the same experimental conditions, was subtracted from the buffer−sample scans, and the baseline was drawn for each scan. The apparent melting temperature (T_m) values were determined from the maximum of each thermogram peak. All experiments were performed in duplicate.

Molecular Docking. The ligand 3D structures were built with the Maestro Build Panel. All the tautomeric and protomeric states at physiological pH (7.4 ± 1.5) were predicted using Epik software implemented in the Ligprep tool.[58,59] The X-ray complex of homodimeric PD-L1 with **1** (PDB code: 5J89) was selected due to the high degree of structural similarity between the co-crystalized ligand and our triazine-based compounds. The receptor was prepared with the aid of the Protein Preparation Wizard panel of Maestro Suite (Schrödinger Release 2019-2: Schrödinger Suite 2019-1),[60] adding the missing hydrogen atoms and removing any water molecule with less than two hydrogen bonds to non-water molecules. In addition, the side chain ionization and tautomeric states were predicted and the H-bonding network of the receptor refined minimizing the position of each hydrogen. The search grid was set around the co-crystallized ligand through the grid generation tool of the Glide 8.1 program.[61−63] Then, docking calculations were performed using Glide 8.1 in its SP variant and employing the OPLS3E force field[61−63] Thus, the top-ranked compounds were selected and visually double checked for a good chemical geometry.

Cell Cultures. Human immortalized keratinocyte cell line HaCaT and NSCLC cell lines PC9 and HCC827 were obtained from the American Type Culture Collection (ATCC). The HaCat cell line was cultured in Dulbecco's modified Eagle's medium (DMEM) (Euroclone) supplemented with 4.5 g/L glucose, 2 mmol/L L-glutamine, 1% antibiotics (100 IU/mL penicillin and 100 μg/ml streptomycin), and 10% fetal bovine serum (FBS) (Euroclone). The PC9 and HCC827 cell lines were cultured in Roswell Park Memorial Institute (RPMI)-1640 medium supplemented with 2 mmol/L L-glutamine, 1% antibiotics (100 IU/mL penicillin and 100 μg/mL streptomycin), and 10% FBS (Euroclone). All cells were cultured at 37 °C in a 5% CO_2 atmosphere.

PBMC Isolation. PBMCs were isolated from the peripheral blood of healthy donors using Ficoll HyPaque (GE Healthcare). Prior to donating blood, volunteers were informed and provided written informed consent for the use of blood samples for scientific research. Blood was diluted with an equal volume of PBS pH-7.2 and added to Ficoll HyPaque solution (2:1 ratio) before centrifugation at 500*g* for 30 min (min) at room temperature in a swinging bucket rotor with a low acceleration speed. The upper layer was aspirated leaving the mononuclear cells at the interphase. Carefully, mononuclear cells were collected by aspiration using a Pasteur pipette and transferred to a new 50 mL tube. Then, the isolated cells were washed twice with PBS and centrifuged at 400*g* for 10 min at 20 °C to remove platelets. PBMCs were re-suspended in complete RPMI 1640 media (fresh RPMI-1640 medium supplemented with 10% FBS, 2 mM L-glutamine, 100 IU/mL penicillin, and 100 μg/mL streptomycin) (Euroclone) and cultured at 37 °C in a 5% CO_2 atmosphere. Cells were counted for *ex vivo* experiments.

Flow Cytometry Analysis. Cells were seeded at a density of 2×10^5 into 6-well plates in DMEM supplemented with 4.5 g/L glucose, 2 mmol/L L-glutamine, 1% antibiotics (100 IU/mL penicillin and 100 μg/mL streptomycin), and 10% FBS. Following 24 h culturing at 37 °C in a 5% CO_2 atmosphere, cells were incubated with 100 IU/mL recombinant human IFN-γ (PeproTech, USA). Untreated cells were used as a control. Following 4 h incubation, cells were collected and cell surface stained utilizing the APC-conjugated PD-L1-specific mouse mAb (clone 29E.2A3) (EXBIO) according to the manufacturer's instruction. APC-conjugated mouse IgG2b (kappa) (clone MPC-11) (EXBIO) was used as an isotype control. Stained cells were analyzed with a BD FACSVerse flow cytometer (BD Biosciences). Data were analyzed using BD FACSuite software.

Cytotoxicity Assay. Cells were seeded at a density of 1×10^4 per well in 96-well plates in DMEM supplemented with supplemented with 4.5 g/L glucose, 2 mmol/L L-glutamine, 1% antibiotics (100 IU/mL penicillin and 100 μg/mL streptomycin), and 10% FBS and treated with the indicated doses of standard pyridine **1** or triazine **10**. Compound **1** was purchased from Selleck Chemicals and used as a control for PD-L1 inhibition. Untreated cells were used as a control. DMSO (vehicle of the drugs) concentration was maintained at 0.02% in all wells. Doses of compounds to be tested were chosen based on their binding affinity to PD-L1. Cell viability was evaluated at the indicated time points, utilizing the Cell Counting Kit-8 (CCK-8) assay (Dojindo Laboratories, Japan) according to the manufacturer's instructions. The absorbance at 450 nm with the reference wavelength at 600 nm was determined by the Sunrise microplate reader (TECAN). Data are expressed as the percent of survival rate of the treated cells as compared to untreated cells. All experiments were performed three independent times in triplicate.

Immunofluorescence Assay. Double-fluorescence staining of PD-L1 was carried out on non-permeabilized PBMCs, PC9 and HCC827 cells. Cells were seeded at a density of 2×10^5 per well in 6-well plates in DMEM supplemented with 4.5 g/L glucose, 2 mmol/L L-glutamine, 1% antibiotics (100 IU/mL penicillin and 100 μg/mL streptomycin), and 10% FBS. Cultured adherent cells were plated on coverslips. All cells were incubated for 8 h with biotinylated triazine derivatives **20** and **21** at 1 μM dosage. PBMCs were processed with cytospin and successively fixed in paraformaldehyde (2% in PBS) at room temperature for 10 min. Cells were then blocked in antiserum goat (5% in PBS) for 1 h at room temperature and then incubated overnight at 4 °C with PD-L1-specific rabbit mAb (Ab 205921) (1:100 dilution) and CD3-specific mouse mAb (Ab17143). Biotinylated triazines **20** and **21** were detected utilizing a streptavidin-FITC-conjugated secondary antibody (Jackson Immuno Research Laboratories) (1:500 dilution). PD-L1 and CD3 expressions were detected utilizing Alexa Fluor-555- and Alexa Fluor-649-conjugated anti-rabbit IgG and anti-mouse IgG1 secondary antibodies (Jackson Immuno Research Laboratories) (1:500 dilution), respectively. Secondary antibodies were incubated for 1 h at room temperature on Coverslips. Secondary antibodies were used in the absence of primary antibodies as negative controls. Then, coverslips were washed with PBS, and cell nuclei were stained with DAPI (1:10 000 dilution). Following three more washes in cold PBS, coverslips were mounted in mowiol 4−88 (Merck-Millipore) on glass slides. Images relative to co-localization analyses of PD-L1 with triazines **20** and **21** were acquired on a laser scanning confocal microscope (TCS SP5; Leica MicroSystems or LSM 510 Meta; Zeiss MicroSystems) equipped with a plan Apo 63X, NA 1.4 oil immersion objective lens. Briefly, the number of co-localized pixels was normalized for the total fluorescent pixels in the image. The degree of co-localization was assessed by calculating the Pearson's correlation coefficient. The mean fluorescence intensity was measured in the region of interest of equal area in control and treated samples.

https://doi.org/10.1021/acs.jmedchem.1c01409
J. Med. Chem. XXXX, XXX, XXX−XXX

Co-Culture of PBMCs with or without NSCLC Cell Lines. Different conditions were evaluated for the tumor cell/PBMC co-culture system (data not shown). PC9 and HCC827 cells were seeded at a density of 2×10^5 per well in 24-well plates in DMEM supplemented with 4.5 g/L glucose, 2 mmol/L L-glutamine, 1% antibiotics (100 IU/mL penicillin and 100 μg/mL streptomycin), and 10% FBS for 24 h and then 2×10^6 PBMCs were added. Subsequently, cells were incubated with pyridine standard **1** and triazine **10** (1 μM). Following 1 h incubation, PBMCs were stimulated with an anti-CD3 (1 μg/mL) and an anti-CD28 (1 μg/mL) (T Cell TransAct human, Miltenyi Biotec). Untreated cancer cells and unstimulated PBMCs were used as controls. All experiments were performed three independent times in triplicate.

Morphological Changes. Following 48 h of co-culturing with PBMCs, the morphology of PC9 and HCC827 cells was assessed using phase-contrast microscopy. Special attention was paid to find signs of cellular damage, such as the disruption of the intercellular junctional complexes, swollen or prominent nuclei, cytoplasmic vacuolization, a shrunken cytosol or rupture of nuclear and plasma membranes.

IFN-γ ELISA. Following 48 h of incubation, IFN-γ levels in the medium harvested from the cultures of PBMCs with cancer cells was measured utilizing the commercially available kit ELISA Max Deluxe Set Human IFN-γ (Biolegend, USA), according to the manufacturer's instructions. Absorbance was measured at 450 nm using a microplate reader (Sunrise, TECAN). Data were collected and analyzed from three independent experiments, each conducted in triplicate.

Annexin V-FITC/PI Assay. The Annexin V-FITC/PI assay was carried out using an Annexin V-FITC Early apoptosis detection kit (Cell Signaling technology) on cells harvested from cultures of PBMCs with cancer cells, in order to differentiate between viable, necrotic, and apoptotic cells according to the manufacturer's instructions. Stained cells were analyzed with a BD FACSVerse flow cytometer (BD Biosciences). Data were analyzed using BD FACSuite software.

Statistical Analysis. Data were analyzed with GraphPad Prism version 6.0 (GraphPad Software, Inc.). Averages, standard deviations, and unpaired *t*-tests were calculated using MS-Excel. Data are shown as mean ± SD of the results obtained in at least three independent experiments. Differences between groups were considered significant when the P value was < 0.05. The asterisk (*) indicates $P < 0.05$.

■ SYNTHESIS

General. Reagent-grade chemicals and solvents were purchased from Sigma-Aldrich or FluoroChem and were used without further purification. Solvents were dried according to standard procedures, and reactions in anhydrous conditions were performed under a nitrogen atmosphere, using a dry nitrogen flux (passage through Drierite—Ca_2SO_4 traps as a drying agent). Purifications were carried out either by flash chromatography on silica gel (particle size 60 Å, 230−400 mesh) or by Biotage C_{18} reverse-phase chromatography [Biotage column KP-C_{18}-HS (12 or 30 g)]. All derivatives had been obtained in high purity (>95%) and characterized by ^{1}H NMR, ^{13}C NMR, and LC−MS.

NMR spectra were recorded at 300 K on Bruker DRX 300 and Bruker AVANCE 400 instruments in $CDCl_3$, CD_3OD, or DMSO-d_6 as solvents at 300 or 400 MHz (^{1}H NMR) or at 75/101 MHz (^{13}C NMR spectra). Signal attributions and coupling constants are given in Hertz and rounded to the nearest 0.1 Hz. High-temperature ^{1}H NMR of compounds **7**, **8**, **10**, and **11** was also performed in order to induce signal coalescence for conformational species.

LC−MS data were collected with a Waters Acquity ultra-performance LC equipped with an Acquity UPLC HSS T3 column (2.1 mm × 50 mm, 1.8 μm) and a SQD detector.

General Procedure A for the Second Nucleophilic Substitution on DCT Derivatives, and the Third Nucleophilic Substitution on TCT Derivatives. A solution of nucleophile (1.2 equiv) and DIPEA (1.5 equiv) in dry CH_3CN was added to a solution of the triazine (1 equiv) in dry CH_3CN under a nitrogen atmosphere. The reaction mixture was heated up to 60−70 °C and stirred for 3−16 h; after reaction completion (TLC monitoring), it was cooled to room temperature and the solvent was evaporated under reduced pressure. Dichloromethane (DCM) was added to the residue and saturated aqueous solution of NH_4Cl was slowly added until neutral pH was achieved. Then, the mixture was extracted with DCM and the collected organic phases were washed with brine, dried over sodium sulfate, filtered, and evaporated under reduced pressure. The crude was purified by flash chromatography or reverse-phase chromatography to afford either a target 2,4-disubstituted triazine from DCT or a 2,4,6-trisubstituted triazine from TCT.

*Synthetic Procedures for 2,4,6-Trisubstituted Cyanobenzyloxy Triazines 7−9. 2,4-Dichloro-6-((2-methyl-[1,1′-biphenyl]-3-yl)methoxy)-1,3,5-triazine (**23**).* A solution of (2-methyl-[1,1′-biphenyl]-3-yl)-methanol (404.2 mg, 2.04 mmol, 1 equiv) and DIPEA (0.430 mL, 2.47 mmol, 1.2 equiv) in dry DCM (10 mL) at −20 °C was added dropwise to a stirred solution of TCT (374.4 mg, 2.03 mmol, 1 equiv) in dry DCM (15 mL) at −20 °C under a nitrogen atmosphere. The reaction mixture was allowed to slowly warm to room temperature, and after reaction completion (3 h, TLC monitoring, eluent mixture: 1:1 *n*-hexane/DCM), the mixture was washed with 1 M aqueous HCl (30 mL) and brine (30 mL). The organic phase was dried over sodium sulfate, filtered, and evaporated under reduced pressure. The crude was purified by flash column chromatography over silica gel (eluent mixture: 1:1 *n*-hexane/DCM) to afford 492 mg of pure dichlorotriazine ether **23** as a white solid (1.43 mmol, 70% yield). ^{1}H NMR (400 MHz, $CDCl_3$): δ 7.48−7.35 (m, 4H, H biphenyl), 7.31−7.27 (m, 4H, H biphenyl), 5.63 (s, 2H, OCH_2), 2.31 (s, 3H, CH_3). ^{13}C NMR (101 MHz, $CDCl_3$): δ 172.7, 171.1, 143.4, 141.7, 135.3, 132.5, 131.3, 129.4, 129.3, 128.3, 127.2, 125.8, 71.0, 16.5. MS (ESI$^+$) m/z: $[M + H]^+$ found, 346.29; calcd for $C_{17}H_{13}Cl_2N_3O$, 345.04.

*3-(((4-Chloro-6-((2-methyl-[1,1′-biphenyl]-3-yl)methoxy)-1,3,5-triazin-2 yl)oxy)methyl)benzonitrile (**24**).* A solution of 3-(hydroxymethyl)-benzonitrile (82.1 mg, 0.616 mmol, 1 eq) and DIPEA (0.125 mL, 0.717 mmol, 1.2 eq) in dry DCM (3 mL) at 0 °C was added to a stirred solution of intermediate **23** (208.8 mg, 0.603 mmol, 1 eq) in dry DCM (4 mL) at 0 °C under a nitrogen atmosphere. The reaction mixture was slowly warmed to room temperature, and after reaction completion (48 h, TLC monitoring, eluent mixture: 8:2 *n*-hexane/EtOAc), the mixture was washed with 1 M aqueous HCl (10 mL) and brine (10 mL). The organic phase was dried over sodium sulfate, filtered, and evaporated under reduced pressure. The crude was purified by flash chromatography over silica gel (eluent mixture: 8:2 *n*-hexane/EtOAc) to afford 165 mg of pure monochlorotriazine diether **24** as a white amorphous solid (0.431 mmol, 70% yield). ^{1}H NMR (400 MHz, $CDCl_3$): δ 7.79 (s, 1H, H2 benzonitrile), 7.72 (d, J = 7.8 Hz, 1H, H6 benzonitrile), 7.68 (d, J = 7.8 Hz, 1H, H4 benzonitrile), 7.54 (t, J = 7.8 Hz, 1H, H5 benzonitrile), 7.48−7.35 (m, 4H, H biphenyl), 7.33−7.27 (m, 4H, H biphenyl), 5.58 (s, 2H, OCH_2), 5.53 (s, 2H, OCH_2), 2.31 (s, 3H, CH_3). ^{13}C NMR (75 MHz, $CDCl_3$): δ 173.0, 172.2, 171.9, 143.3, 141.8, 136.3, 135.1, 133.1, 132.5, 132.4, 131.7, 131.0, 129.7, 129.4, 129.1, 128.3, 127.1, 125.7, 118.4, 113.1, 70.1, 69.2, 16.5. MS (ESI$^+$) m/z: $[M + H]^+$ found, 443.35; calcd for $C_{25}H_{19}ClN_4O_2$, 442.12.

https://doi.org/10.1021/acs.jmedchem.1c01409
J. Med. Chem. XXXX, XXX, XXX−XXX

*N-(2-((4-((3-Cyanobenzyl)oxy)-6-((2-methyl-[1,1′-biphenyl]-3-yl)methoxy)-1,3,5-triazin-2-yl)amino)ethyl)acetamide (**7**).* Target trisubstituted triazine amide **7** was synthesized according to general procedure **A**, starting from intermediate **24** (82.4 mg, 0.185 mmol, 1 equiv), *N*-(2-aminoethyl)-acetamide (0.017 mL, 0.185 mmol, 1 equiv), and DIPEA (0.040 mL, 0.229 mmol, 1.2 equiv) in dry CH_3CN (10 mL) at 70 °C for 16 h. The crude was purified by flash chromatography over silica gel (eluent mixture: 95:5 DCM/MeOH) to afford 68.1 mg of pure target **7** as a white amorphous solid (0.133 mmol, 72% yield). ^{1}H NMR (400 MHz, DMSO-d_6, some signals highlighted as *in the text are split due to the presence of two atropisomers in an unknown ratio): δ 8.00−7.90 (m, 3H, H2 and H6 benzonitrile, NH), 7.82−7.76 (m, 2H, H4 and H5 benzonitrile), 7.60 (t, J = 7.8 Hz, 1H, NH), 7.46−7.35 (m, 4H, biphenyl), 7.31−7.18 (m, 4H, H biphenyl), 5.42*, 5.41* (2s, 2H, OCH_2), 5.37*, 5.36* (2s, 2H, OCH_2), 3.33−3.30 (m, 2H, NCH_2), 3.19−3.15 (m, 2H, NCH_2), 2.18*, 2.16* (2s, 3H, CH_3), 1.79*, 1.77* (2s, 3H, $COCH_3$). ^{13}C NMR (101 MHz, DMSO-d_6, some signals are split due to the presence of two atropisomers in an unknown ratio): δ: 171.5, 171.3, 171.1, 170.9, 169.4, 167.7, 142.2, 141.3, 138.2, 138.1, 134.9, 133.9, 133.7, 132.8, 131.8, 131.6, 131.5, 129.7, 129.1, 128.4, 128.2, 128.0, 127.0, 125.6, 118.6, 111.4, 67.1, 66.9, 66.7, 38.0, 22.6, 15.8. MS (ESI$^+$) m/z: [M + H]$^+$ found 509.47, calculated for $C_{29}H_{28}N_6O_3$ 508.22.

*Methyl (4-((3-Cyanobenzyl)oxy)-6-((2-methyl-[1,1′-biphenyl]-3-yl)methoxy)-1,3,5-triazin-2-yl)-L-histidinate (**8**).* Target trisubstituted triazine ester **8** was synthesized according to general procedure **A**, starting from intermediate **24** (175.0 mg, 0.393 mmol, 1 equiv), L-histidine methyl ester·dihydrochloride (95.0 mg, 0,393 mmol, 1 equiv), and N,N-diisopropylethylamine (DIPEA) (0.260 mL, 1.492 mmol, 3.7 equiv) in dry CH_3CN (15 mL) at 70 °C for 5 h. The crude was purified by Biotage reverse-phase chromatography (eluent mixture: CH_3CN/H_2O, gradient from 20 to 100% CH_3CN) to afford 140 mg of pure target **8** as a white amorphous solid (0.244 mmol, 62% yield). ^{1}H NMR (400 MHz, CD_3OD, some signals highlighted as *in the text are split due to the presence of two atropisomers in an unknown ratio): δ 7.82−7.79 (m, 1H, H2 benzonitrile), 7.75−7.71 (m, 1H, H4 benzonitrile), 7.68−7.66 (m, 1H, H6 benzonitrile), 7.58 (s, 1H, H His), 7.56−7.52 (m, 1H, H5 benzonitrile), 7.42−7.31 (m, 4H, biphenyl), 7.26−7.15 (m, 4H, biphenyl), 6.87 (m, 1H, H His), 5.48−5.36 (m, 4H, OCH_2), 4.90−4.81 (m, 1H, Hα His), 3.68*, 3.66* (2s, 3H, $COOCH_3$), 3.23−3.05 (m, 2H, Hβ His), 2.21*, 2.20* (2s, 3H, CH_3). ^{13}C NMR (101 MHz, DMSO-d_6, some signals are split due to the presence of two atropisomers in an unknown ratio): δ 172.2, 171.3, 171.1, 167.5, 142.2, 141.3, 138.0, 135.1, 134.8, 133.8, 132.9, 131.8, 131.6, 131.5, 129.8, 129.7, 129.2, 128.2, 128.1, 127.0, 125.6, 118.6, 111.5, 67.2, 67.0, 54.4, 54.3, 52.0, 15.8. MS (ESI$^+$) m/z: [M + H]$^+$ found, 576.53; calcd for $C_{32}H_{29}N_7O_4$, 575.23.

*(4-((3-Cyanobenzyl)oxy)-6-((2-methyl-[1,1′-biphenyl]-3-yl)methoxy)-1,3,5-triazin-2-yl)-L-histidine (**9**).* Solid LiOH·H_2O (7 mg, 0.166 mmol, 3 equiv) was added under stirring to a solution of target trisubstituted triazine ester **8** (33 mg, 0.0573 mmol, 1 equiv) in 3:1 THF/H_2O (4 mL). The resulting mixture was stirred at room temperature for 3 h. After reaction completion (TLC monitoring, eluent mixture: 9:1 DCM/MeOH), 0.5 M aqueous HCl was added until pH ≈ 3, then the mixture was extracted with EtOAc (5 × 20 mL). The collected organic layers were washed with brine (10 mL), dried over sodium sulfate, filtered, and evaporated under reduced pressure affording 42.0 mg of the crude white solid. The crude was purified by Biotage reverse-phase chromatography (eluent mixture: CH_3CN/H_2O, gradient from 20% to 100% CH_3CN), affording 19.0 mg of pure target trisubstituted triazine carboxylate **9** as a white amorphous solid (0.0344 mmol, 60% yield). ^{1}H NMR (400 MHz, CD_3OD, some signals highlighted as *in the text are split due to the presence of two atropisomers in an unknown ratio): δ 8.27 (s, 1H, H His), 7.84 (m, 1H, H2 benzonitrile), 7.78−7.74 (m, 1H, H6 benzonitrile), 7.70−7.68 (m, 1H, H4 benzonitrile), 7.59−7.54 (m, 1H, H5 benzonitrile), 7.44−7.32 (m, 4H, H biphenyl), 7.28−7.17 (m, 4H, H biphenyl), 7.10 (m, 1H, H His), 5.49−5.43 (m, 4H, OCH_2), 4.73−4.65 (dt, J = 19.3, 5.8 Hz, 1H, Hα His), 3.40−3.15 (m, 2H, Hβ His), 2.24*, 2.22* (2s, 3H, CH_3). ^{13}C NMR (101 MHz, DMSO-d_6, some signals are split due to the presence of two atropisomers in an unknown ratio): δ 173.1, 171.3, 171.1, 171.0, 167.5, 142.2, 141.3, 138.0, 134.8, 134.7, 133.9, 133.8, 133.0, 132.9, 131.8, 131.7, 131.6, 129.7, 129.2, 128.2, 127.0, 125.6, 118.6, 111.5, 67.2, 67.0, 66.9, 54.3, 28.5, 15.9. MS (ESI$^+$): m/z [M + H]$^+$ found, 562.49; calcd for $C_{31}H_{27}N_7O_4$, 561.21.

*Synthetic Procedures for 2,4-Disubstituted Triazines 10−12. 2-Chloro-4-((2-methyl-[1,1′-biphenyl]-3-yl)methoxy)-1,3,5-Triazine (**25**).* A solution of (2-methyl-[1,1′-biphenyl]-3-yl)-methanol (826.0 mg, 4.167 mmol, 1 equiv) and DIPEA (0.841 mL, 4.834 mmol, 1.2 equiv) in dry DCM (4 mL) at −20 °C was added dropwise to a stirred solution of DCT (625.0 mg, 4.167 mmol, 1 equiv) in dry DCM (6 mL) at −20 °C under a nitrogen atmosphere. The reaction mixture was slowly warmed to room temperature, and after reaction completion (5 h, TLC monitoring, eluent mixture: 8:2 *n*-hexane/EtOAc), the mixture was washed with 1 M aqueous HCl (10 mL) and brine (10 mL). The organic phase was dried over sodium sulfate, filtered, and evaporated under reduced pressure. The crude was purified by flash chromatography over silica gel (eluent mixture: 9:1 *n*-hexane/EtOAc) to afford 318 mg of pure chlorotriazine ether **25** (1.019 mmol) as a white solid (1.25 mmol, 30% yield). ^{1}H NMR (400 MHz, $CDCl_3$): δ 8.75 (s, 1H, H triazine), 7.47−7.33 (m, 4H, H biphenyl), 7.30−7.25 (m, 4H, H biphenyl), 5.60 (s, 2H, OCH_2), 2.30 (s, 3H, CH_3). ^{13}C NMR (101 MHz, $CDCl_3$) δ: 172.5, 170.7, 169.1, 143.3, 141.8, 135.1, 133.1, 131.0, 129.5, 129.1, 128.3, 127.1, 125.7, 70.0, 16.5. MS (ESI$^+$) m/z: [M + H]$^+$ found, 312.18; calcd for $C_{17}H_{14}ClN_3O$, 311.08.

*N-(2-((4-((2-Methyl-[1,1′-biphenyl]-3-yl) methoxy)-1,3,5-triazin-2-yl)amino)ethyl)acetamide (**10**).* Target disubstituted triazine amide **10** was synthesized according to general procedure **A**, starting from intermediate **25** (300.0 mg, 0.96 mmol, 1 equiv), *N*-(2-aminoethyl)-acetamide (0.120 mL, 1.25 mmol, 1.3 eq), and DIPEA (0.250 mL, 1.44 mmol, 1.5 equiv) in dry CH_3CN (3.2 mL) at 70 °C for 4 h. The crude was purified by flash chromatography over silica gel (eluent mixture: 9:1 DCM/MeOH) to afford 289.0 mg of pure target **10** as a white amorphous solid (0.77 mmol, 80% yield). ^{1}H NMR (400 MHz, $CDCl_3$, some signals highlighted as *in the text are split due to the presence of two atropisomers in an unknown ratio): δ 8.41*, 8.32* (2s, 1H, H triazine), 7.43−7.33 (m, 4H, H biphenyl), 7.30−7.22 (m, 4H, H biphenyl), 6.11−5.96 (m, 2H, NH), 5.48*, 5.44* (2s, 2H, OCH_2), 3.61−3.57 (m, 2H, NCH_2), 3.48−3.46 (m, 2H, NCH_2), 2.27*, 2.26* (2s, 3H, CH_3), 1.97*, 1.93* (2s, 3H, $COCH_3$). ^{13}C NMR (101 MHz, DMSO-d_6, some signals are split due to the presence of two atropisomers in an unknown ratio): δ 169.7, 169.5, 169.4, 166.5, 166.4, 142.2, 141.4, 135.0, 134.9, 133.9, 129.8, 129.7, 129.2, 128.4, 128.3,

https://doi.org/10.1021/acs.jmedchem.1c01409
J. Med. Chem. XXXX, XXX, XXX−XXX

128.0, 127.0, 125.6, 66.9, 66.7, 37.9, 22.6, 15.8. MS (ESI$^+$) m/z: [M + H]$^+$ found, 378.39; calcd for $C_{21}H_{23}N_5O_2$, 377.18.

*Methyl (4-((2-Methyl-[1,1′-biphenyl]-3-yl)methoxy)-1,3,5-triazin-2-yl)-L-histidinate (**11**).* Target disubstituted triazine ester **11** was synthesized according to general procedure **A**, using intermediate **25** (48 mg, 0.154 mmol, 1 equiv), L-histidine methyl ester·dihydrochloride (41 mg, 0.169 mmol, 1.1 equiv), and DIPEA (0.093 mL, 0.539 mmol, 3.5 equiv) in dry CH_3CN (10 mL) at 70 °C for 5 h. The crude was purified by Biotage reverse-phase chromatography (eluent mixture: CH_3CN/H_2O, gradient from 20% to 100% of CH_3CN) to afford 40.0 mg of pure target **11** as a white amorphous solid (0.0909 mmol, 59% yield). ^{1}H NMR (400 MHz, $CDCl_3$, some signals highlighted as *in the text are split due to the presence of two atropisomers in an unknown ratio): δ 8.39*, 8.33* (2s, 1H, H triazine), 7.59*, 7.55* (2s, 1H, H His), 7.43−7.32 (m, 4H, H biphenyl), 7.31−7.22 (m, 5H, H biphenyl, NH His), 6.84*, 6.81* (2s, 1H, H His), 5.44 (s, 2H, OCH_2), 5.01−4.95 (m, 1H, Hα His), 3.73*, 3.69* (2s, 3H, $COOCH_3$), 3.24−3.19 (m, 2H, Hβ His), 2.26 (s, 3H, CH_3). ^{13}C NMR (75 MHz, $CDCl_3$, some signals are split due to the presence of two atropisomers in an unknown ratio): δ 172.2, 171.7, 170.1, 166.4, 166.0, 143.1, 141.9, 134.6, 134.4, 130.4, 129.4, 128.5, 128.2, 127.0, 125.6, 68.1, 55.1, 54.1, 52.5, 29.3, 16.4. MS (ESI$^+$) m/z: [M + H]$^+$ found, 445.44; calcd for $C_{24}H_{24}N_6O_3$, 444.19.

*(4-((2-Methyl-[1,1′-biphenyl]-3-yl)methoxy)-1,3,5-triazin-2-yl)-L-histidine (**12**).* Solid LiOH·H_2O (6 mg, 0.139 mmol, 2 equiv) was added under stirring to a solution of target disubstituted triazine ester **11** (31 mg, 0.0697 mmol, 1 equiv) in 3:1 THF/H_2O (4 mL). The resulting mixture was stirred at room temperature for 2.5 h. After reaction completion (TLC monitoring, eluent mixture: 9:1 DCM/MeOH), 0.5 M aqueous HCl was added dropwise until pH ≈ 3, and then the mixture was extracted with EtOAc (4 × 5 mL). The collected organic layers were washed with brine (10 mL), dried over sodium sulfate, filtered, and evaporated under reduced pressure affording 29.0 mg of a crude white solid. The crude was purified by Biotage reverse-phase chromatography (eluent mixture: CH_3CN/H_2O, gradient from 20 to 100% CH_3CN), affording 18.0 mg of pure target disubstituted triazine carboxylate **12** as a white amorphous solid (0.0418 mmol, 60% yield). ^{1}H NMR (400 MHz, CD_3OD, some signals highlighted as *in the text are split due to the presence of two atropisomers in an unknown ratio): δ 8.45*, 8.39* (2s, 1H, H triazine), 8.28*, 8.23* (2s, 1H, H His), 7.42−7.31 (m, 4H, H biphenyl), 7.26−7.15 (m, 5H, H biphenyl, H His), 5.48−5.43 (m, 2H, OCH_2), 4.76−4.72 (m, 1H, Hα His), 3.40−3.20 (m, 2H, Hβ His), 2.23*, 2.20* (2s, 3H, CH_3). ^{13}C NMR (101 MHz, DMSO-d_6, some signals are split due to the presence of two atropisomers in an unknown ratio): δ 172.9, 169.4, 166.2, 142.2, 141.3, 134.8, 133.9, 129.8, 129.2, 128.4, 128.2, 128.1, 127.0, 125.6, 66.9, 54.0, 15.8. MS (ESI$^+$) m/z: [M + H]$^+$ found, 431.53; calcd for $C_{23}H_{22}N_6O_3$, 430.18.

*Synthetic Procedures for Polar Chain-Modified Disubstituted Triazines **13**−**15**. N-(3-((4-((2-Methyl-[1,1′-biphenyl]-3-yl)methoxy)-1,3,5-triazin-2-yl)amino)propyl)acetamide (**13**).* Target, homologated disubstituted triazine amide **13** was synthesized according to general procedure **A**, starting from intermediate **25** (150 mg, 0.480 mmol, 1 equiv), *N*-acetyl propylenediamine (77 mg, 0.624 mmol, 1.3 equiv), and DIPEA (125 μL, 0.720 mmol, 1.5 equiv) in dry THF (1.5 mL) at 70 °C for 6 h. The crude was purified by flash chromatography (eluent mixture: 95:5 DCM/MeOH), affording 82.0 mg of pure target **13** as a white solid (0.210 mmol, 55% yield). ^{1}H NMR (400 MHz, $CDCl_3$, some signals highlighted as *in the text are split due to the presence of two atropisomers in an unknown ratio): δ 8.42*, 8.36* (2s, 1H, H triazine), 7.44−7.32 (m, 4H, H biphenyl), 7.29−7.22 (m, 4H, H biphenyl), 6.56−6.29 (m, 2H, NH), 5.52*, 5.45* (2s, 2H, OCH_2), 3.55−3.54 (m, 2H, NCH_2), 3.33−3.32 (m, 2H, NCH_2), 2.27*, 2.26* (2s, 3H, CH_3), 2.02*, 1.97* (2s, 3H, $COCH_3$), 1.83−1.73 (m, 2H, CH_2). ^{13}C NMR (101 MHz, $CDCl_3$, some signals are split due to the presence of two atropisomers in an unknown ratio): δ 171.0, 141.9, 134.8, 130.7, 130.4, 129.5, 129.4, 128.8, 128.5, 128.3, 128.2, 127.1, 127.0, 125.9, 125.7, 125.6, 68.7, 45.7, 38.1, 36.5, 35.9, 29.8, 23.5, 23.4, 16.5, 16.4. MS (ESI$^+$) m/z: [M + H]$^+$ found, 392.35; calcd for $C_{22}H_{25}N_5O_2$, 391.20.

*N-(2-((4-((2-Methyl-[1,1′-biphenyl]-3-yl)methoxy)-1,3,5-triazin-2-yl)amino)ethyl)methanesulfonamide (**14**).* Target disubstituted triazine methylsulfonamide **14** was synthesized according to general procedure **A**, using intermediate **25** (104 mg, 0.320 mmol, 1 equiv), *N*-(2-aminoethyl)-methanesulfonamide (50 mg, 0.353 mmol, 1.1 equiv), and DIPEA (0.073 mL, 0.416 mmol, 1.3 equiv) in dry THF (2 mL) at 70 °C for 6 h. The crude solid was purified by flash chromatography (eluent mixture: 95:5 DCM/MeOH), affording 122 mg of pure target **14** as a white solid (0.295 mmol, 92% yield). ^{1}H NMR (400 MHz, $CDCl_3$, some signals highlighted as *in the text are split due to the presence of two atropisomers in an unknown ratio): δ 8.38*, 8.35* (2s, 1H, H triazine), 7.40−7.30 (m, 4H, H biphenyl), 7.26−7.20 (m, 4H, H biphenyl), 6,71*, 5.90*, 5.78* (3m, 2H, NH), 5.46*, 5.41* (2s, 2H, OCH_2), 3.64−3.57 (m, 2H, NCH_2), 3.32−3.27 (m, 2H, NCH_2), 2.90*, 2.89* (2s, 3H, SO_2CH_3), 2.23*, 2.22* (2s, 3H, CH_3). ^{13}C NMR (101 MHz, $CDCl_3$, some signals are split due to the presence of two atropisomers in an unknown ratio): δ 169.7, 167.0, 143.1, 141.9, 134.8, 134.3, 133.7, 130.6, 129.4, 128.8, 128.6, 128.2, 127.1, 125.7, 68.9, 68.2, 43.0, 42.4, 41.4, 40.5, 16.4. MS (ESI$^+$): m/z [M + H]$^+$ found, 414.44; calcd for $C_{20}H_{23}N_5O_3S$, 413.15.

*2-((4-((2-Methyl-[1,1′-biphenyl]-3-yl)methoxy)-1,3,5-triazin-2-yl)amino)ethane-1-sulfonamide (**15**).* Target disubstituted triazine sulfonamide **15** was synthesized according to general procedure **A**, starting from intermediate **25** (96 mg, 0.308 mmol, 1 equiv), 2-aminoethanesulfonamide (43 mg, 0.338 mmol, 1.1 equiv), and DIPEA (0.070 mL, 0.401 mmol, 1.3 equiv) in dry THF (3 mL) at 70 °C for 6 h. The crude was purified by flash chromatography (eluent mixture: DCM/MeOH from 98:2 to 95:5), affording 114 mg of pure target **15** as a white solid (0.286 mmol, 93% yield). ^{1}H NMR (400 MHz, $CDCl_3$, some signals highlighted as *in the text are split due to the presence of two atropisomers in an unknown ratio): δ 8.26*, 8.19* (s, 1H, triazine), 7.28−7.07 (m, 8H, H biphenyl), 6.66−6.62 (m, 1H, NH), 5.74 (br s, 2H, SO_2NH_2), 5.32*, 5.28* (2s, 2H, OCH_2), 3.80−3.78 (m, 2H, NCH_2), 3.29−3.26 (m, 2H, NCH_2), 2.11*, 2.09* (2s, 3H, CH_3). ^{13}C NMR (101 MHz, $CDCl_3$, some signals are split due to the presence of two atropisomers in an unknown ratio): δ 170.0, 169.8, 166.6, 166.2, 143.1, 141.4, 134.7, 134.5, 134.3, 134.1, 130.8, 130.5, 129.4, 129.2, 128.7, 128.2, 127.1, 125.9, 125.7, 68.6, 68.2, 53.7, 45.7, 36.1, 16.4. MS (ESI$^+$) m/z: [M + H]$^+$ found, 400.39, calcd for $C_{19}H_{21}N_5O_3S$, 399.14.

*Synthetic Procedures for Trisubstituted Triazines Bearing a Small Third Substituent (**16**−**18**). N-(2-((4-Chloro-6-((2-methyl-[1,1′-biphenyl]-3-yl)methoxy)-1,3,5-triazin-2 yl)-amino)ethyl)acetamide (**16**).* A solution of *N*-(2-aminoethyl)-acetamide (85.7 mg, 0.84 mmol, 1 equiv) and DIPEA (0.176

https://doi.org/10.1021/acs.jmedchem.1c01409
J. Med. Chem. XXXX, XXX, XXX−XXX

mL, 1.01 mmol, 1.2 equiv) in dry DCM (4 mL) at −20 °C was added dropwise to a stirred solution of intermediate **23** (291 mg, 0.84 mmol, 1 equiv) in dry DCM (4 mL) at −20 °C under a nitrogen atmosphere. The reaction mixture was slowly warmed to room temperature, and after reaction completion (4 h, TLC monitoring, eluent mixture: 9:1 DCM/MeOH), the mixture was washed with 1 M aqueous HCl (10 mL) and brine (10 mL). The organic phase was dried over sodium sulfate, filtered, and evaporated under reduced pressure. The crude was purified by flash chromatography over silica gel (eluent mixture: 9:1 DCM/MeOH) to afford 154 mg of pure target trisubstituted chlorotriazine amide **16** as a white solid (0.454 mmol, 45% yield). ^{1}H NMR (400 MHz, $CDCl_3$, some signals highlighted as *in the text are split due to the presence of two atropisomers in an unknown ratio): δ 7.44−7.32 (m, 4H, H biphenyl), 7.29−7.23 (m, 4H, H biphenyl), 6.70*, 6.54* (2m, 1H, NH), 6.17*, 6.97* (2m, 1H, NH), 5.49*, 5.45* (2s, 2H, OCH_2), 3.62−3.58 (m, 2H, NCH_2), 3.50−3.42 (m, 2H, NCH_2), 2.27*, 2.26* (2s, 3H, CH_3), 1.98*, 1.92* (2s, 3H, $COCH_3$). ^{13}C NMR (101 MHz, $CDCl_3$, some signals are split due to the presence of two atropisomers in an unknown ratio): δ 171.4, 171.2, 170.7, 170.4, 170.2, 167.3, 143.1, 141.8, 134.9, 133.9, 130.6, 129.4, 128.9, 128.2, 127.0, 125.6, 69.1, 68.9, 53.6, 41.7, 41.5, 39.7, 39.2, 23.1, 16.4. MS (ESI$^+$) m/z: [M + H]$^+$ found, 412.34; calcd for $C_{21}H_{22}ClN_5O_2$, 411.15.

*N-(2-((4-Hydroxy-6-((2-methyl-[1,1′-biphenyl]-3-yl)-methoxy)-1,3,5-triazin-2-yl)amino)ethyl)acetamide (**17**).* Solid sodium acetate (24.0 mg, 0.293 mmol, 2.0 equiv) and *N*-methylmorpholine (15.0 μL, 0.136 mmol, 1.1 equiv) were sequentially added to a stirred solution of target trisubstituted chlorotriazine **16** (51.0 mg, 0.124 mmol, 1.0 equiv) in 4:1*i*-PrOH/H_2O (0.441 mL) at 0 °C. The resulting mixture was stirred under a nitrogen atmosphere, monitoring by TLC (eluent mixture: 9:1 DCM/MeOH). After 6 h at 0 °C, the reaction was gradually warmed to room temperature, left overnight stirring, and then gently warmed to 40 °C (6 h) and finally to 50 °C (12 h). Then, the reaction mixture was diluted with water (10 mL) and extracted with DCM (3 × 5 mL). The collected organic phases were washed with brine (2 × 5 mL), dried over sodium sulfate, and evaporated under reduced pressure, obtaining a crude white solid (25 mg). The crude was purified by flash chromatography (eluent mixture: 9:1 DCM/MeOH), affording 14.6 mg of pure target trisubstituted hydroxytriazine amide **17** as a white solid (0.0408 mmol, 30% yield). ^{1}H NMR (400 MHz, DMSO-d_6, some signals highlighted as *in the text are split due to the presence of two atropisomers in an unknown ratio): δ 11.50*, 10.95* (2 bs, 1H, OH/NH triazine), 7.93 (t, J = 5.6 Hz, 1H, NH), 7.47−7.36 (m, 4H, H biphenyl), 7.31−7.19 (m, 4H, H biphenyl), 5.40*, 5.34* (2s, 2H, OCH_2), 3.29−3.34 (m, 2H, NCH_2), 3.19−3.15 (m, 2H, NCH_2), 2.18 (s, 3H, CH_3), 1.80*, 1.78* (2s, 3H, $COCH_3$). ^{13}C NMR (101 MHz, DMSO-d_6, some signals are split due to the presence of two atropisomers in an unknown ratio): δ 169.4, 142.2, 141.3, 133.8, 129.7, 129.0, 128.2, 126.9, 125.5, 67.1, 38.0, 22.5, 15.7. MS (ESI$^+$) m/z: [M + H]$^+$ found, 394.31; calcd for $C_{21}H_{23}N_5O_3$, 393.18.

*2,4-Dichloro-6-methoxy-1,3,5-triazine (**26**).* A suspension of $NaHCO_3$ (46.0 mg, 0.548 mmol, 1.0 equiv) and MeOH (1.0 mL, 24.72 mmol, 45 equiv) in dry DCM (3.0 mL) was slowly added to a stirred solution of TCT (100 mg, 0.542 mmol, 1.0 equiv) in dry DCM (2.0 mL), under a nitrogen atmosphere at room temperature. The reaction mixture was stirred for 30 min monitoring by TLC (eluent mixture: 8:2 *n*-hexane/EtOAc). After reaction completion, the mixture was diluted with water (10 mL) and extracted with DCM (3 × 5 mL). The collected organic phases were washed with brine (2 × 5 mL) and dried over sodium sulfate. The solvent was evaporated under reduced pressure, obtaining 71.0 mg of dichloromethoxy triazine **26**, a white solid (0.396 mmol, 73% yield), that was used without any further purification. ^{1}H NMR (400 MHz, $CDCl_3$): δ 4.13 (s, 3H, OCH_3).

*2-Chloro-4-methoxy-6-((2-methyl-[1,1′-biphenyl]-3-yl)-methoxy)-1,3,5-triazine (**27**).* A solution of (2-methyl-[1,1′-biphenyl]-3-yl)-methanol (78 mg, 0.394 mmol, 1 equiv) and DIPEA (0.082 mL, 0.473 mmol, 1.2 equiv) in dry DCM (2 mL) at 0 °C was added to a stirred solution of intermediate **26** (71 mg, 0.394 mmol, 1 equiv) in dry DCM (3 mL) at 0 °C under a nitrogen atmosphere. The reaction mixture was slowly warmed to room temperature, and after reaction completion (4 h, TLC monitoring, eluent mixture: 8:2 *n*-hexane/EtOAc), the mixture was washed with 1 M aqueous HCl (5 mL) and brine (5 mL). The organic phase was dried over sodium sulfate, filtered, and evaporated under reduced pressure. The crude was purified by flash chromatography over silica gel (eluent mixture: 8:2 *n*-hexane/EtOAc) to afford 88.0 mg of pure chloromethoxy triazine ether **27** as a white solid (0.256 mmol, 65% yield). ^{1}H NMR (400 MHz, $CDCl_3$): δ 7.46−7.33 (m, 4H, H biphenyl), 7.30−7.23 (m, 4H, H biphenyl), 5.56 (s, 2H, OCH_2), 4.08 (s, 3H, OCH_3), 2.28 (s, 3H, CH_3). ^{13}C NMR (101 MHz, $CDCl_3$): δ 172.8, 172.2, 143.6, 141.9, 135.1, 133.3, 130.9, 129.5, 129.2, 129.1, 128.3, 127.1, 125.7, 69.9, 56.3, 16.5. MS (ESI$^+$) m/z: [M + H]$^+$ found, 342.16; calcd for $C_{18}H_{16}ClN_3O_2$, 341.09.

*N-(2-((4-Methoxy-6-((2-methyl-[1,1′-biphenyl]-3-yl)-methoxy)-1,3,5-triazin-2-yl)amino)ethyl)acetamide (**18**).* Target trisubstituted methoxy triazine amide **18** was synthesized according to general procedure **A**, starting from intermediate **27** (20.0 mg, 0.059 mmol, 1 equiv), *N*-(2-aminoethyl)acetamide (9.0 mg, 0.089 mmol, 1 equiv), and DIPEA (0.018 mL, 0.1 mmol, 1.7 equiv) in dry CH_3CN (5 mL) at 70 °C for 5 h. The crude was purified by flash chromatography over silica gel (eluent mixture: 98:2 DCM/MeOH) to afford 16.6 mg of pure compound **18** as a white solid (0.041 mmol, 69% yield). ^{1}H NMR (400 MHz, $CDCl_3$, some signals highlighted as *in the text are split due to the presence of two atropisomers in an unknown ratio): δ 7.43−7.33 (m, 4H, H biphenyl), 7.29−7.23 (m, 4H, H biphenyl), 6.66−6.61 (m, 1H, NH), 6.20 (m, 1H, NH), 5.49*, 5.46* (2s, 2H, OCH_2), 4.01*, 3.97* (2s, 3H, OCH_3), 3.60−3.59 (m, 2H, NCH_2), 3.48−4.44 (m, 2H, NCH_2), 2.27*, 2.26* (2s, 3H, CH_3), 1.96*, 1.93* (2s, 3H, $COCH_3$). ^{13}C NMR (101 MHz, $CDCl_3$, some signals are split due to the presence of two atropisomers in an unknown ratio): δ 170.7, 142.8, 134.6, 130.3, 129.2, 128.7, 127.9, 126.7, 125.3, 68.5, 68.4, 54.9, 40.9, 39.5, 23.1, 16.2. MS (ESI$^+$) m/z: [M + H]$^+$ found, 408.36; calcd for $C_{22}H_{25}N_5O_3$, 407.20.

*Synthetic Procedures for Trisubstituted Methyl Triazine **19**.*

*2-Chloro-4-methyl-6-((2-methyl-[1,1′-biphenyl]-3-yl)-methoxy)-1,3,5-triazine (**28**).* A solution of (2-methyl-[1,1′-biphenyl]-3-yl)-methanol (248.0 mg, 1.251 mmol, 1.0 equiv) and DIPEA (235.0 μL, 1.355 mmol, 1.1 equiv) in dry CH_3CN (3.0 mL) was added dropwise to a stirred solution of 2,4-dichloro-6-methyl-1,3,5-triazine (202 mg, 1.232 mmol, 1.0 equiv) in dry CH_3CN (2 mL), under a nitrogen atmosphere at room temperature. The reaction mixture was stirred at 40 °C for 6 h and overnight at room temperature, monitoring by TLC (eluent mixture: *n*-hexane/EtOAc 9:1). The reaction was then stopped, due to evidence of degradation side products. The

https://doi.org/10.1021/acs.jmedchem.1c01409
J. Med. Chem. XXXX, XXX, XXX−XXX

solvent was evaporated under reduced pressure, and the residue was diluted with water (10 mL). The mixture was extracted with DCM (3 × 5 mL). The collected organic phases were washed with brine (2 × 5 mL), dried over sodium sulfate, filtered, and the solvent was evaporated under reduced pressure, obtaining a white solid residue (371.3 mg). The crude was purified by flash chromatography (eluent mixture: 9:1 *n*-hexane/EtOAc), affording 88.8 mg of pure trisubstituted chloromethyl triazine ether **28** as a white solid (0.298 mmol, 22% yield). ^{1}H NMR (400 MHz, $CDCl_3$): δ 7.47−7.33 (m, 4H, H biphenyl), 7.30−7.25 (m, 4H, H biphenyl), 5.57 (s, 2H, OCH_2), 2.61 (s, 3H, CH_3 triazine), 2.29 (s, 3H, CH_3). ^{13}C NMR (101 MHz, $CDCl_3$): δ 180.5, 142.9, 141.6, 134.8, 133.0, 130.6, 129.1, 128.8, 127.9, 126.8, 125.4, 69.4, 25.3, 16.2. MS (ESI$^+$) *m*/*z*: [M + H]$^+$ found, 326.22; calcd for $C_{18}H_{16}ClN_3O$, 325.10.

*N-(2-((4-Methyl-6-((2-methyl-[1,1′-biphenyl]-3-yl)-methoxy)-1,3,5-triazin-2-yl)amino)ethyl)acetamide (**19**).* Target trisubstituted methyl triazine amide **19** was synthesized according to general procedure **A**, starting from intermediate **28** (83.0 mg, 0.255 mmol, 1 equiv), *N*-(2-aminoethyl)-acetamide (0.037 mL, 0.382 mmol, 1.5 equiv), and DIPEA (0.075 mL, 0.433 mmol, 1.7 equiv) in dry CH_3CN (5 mL) at 70 °C for 24 h. The crude was purified by flash chromatography over silica gel (eluent mixture: 95:5 DCM/MeOH) to afford 48.2 mg of pure target **19** as a white solid (0.122 mmol, 48% yield). ^{1}H NMR (400 MHz, $CDCl_3$, some signals highlighted as *in the text are split due to the presence of two atropisomers in an unknown ratio): δ 7.48−7.37 (m, 4H, H biphenyl), 7.33−7.27 (m, 4H, H biphenyl), 6.63−6.57 (m, 1H, NH), 6.44−6.30 (m, 1H, NH), 5.51*, 5.47* (2s, 2H, OCH_2), 3.63−3.62 (m, 2H, NCH_2), 3.49−3.46 (m, 2H, NCH_2), 2.46*, 2.41* (2s, 3H, CH_3 triazine), 2.32*, 2.31* (2s, 3H, CH_3), 1.98*, 1.91* (2s, 3H, $COCH_3$). ^{13}C NMR (101 MHz, $CDCl_3$, some signals are split due to the presence of two atropisomers in an unknown ratio): δ 178.4, 177.6, 171.0, 167.6, 143.0, 142.0, 134.7, 130.3, 129.4, 128.7, 128.2, 127.0, 125.5, 67.9, 67.7, 40.9, 40.5, 39.7, 25.7, 25.4, 23.2, 16.4. MS (ESI$^+$) *m*/*z*: [M + H]$^+$ found, 392.44; calcd for $C_{22}H_{25}N_5O_2$, 391.20.

*Synthetic Procedures for Biotinylated Trisubstituted Triazine **20**. 4-Chloro-6-((2-methyl-[1,1′-biphenyl]-3-yl)-methoxy)-N-(prop-2-yn-1-yl)-1,3,5-triazin-2-amine (**29**).* A solution of propargylamine (27 μL, 0.433 mmol, 1 equiv) and DIPEA (90 μL, 0.520 mmol, 1.2 equiv) in dry DCM (2.3 mL) was added at −20 °C and under a nitrogen atmosphere to a solution of intermediate **23** (150.3 mg, 0.433 mmol, 1 equiv) in dry DCM (2.3 mL). The reaction mixture was stirred at −20 °C for 1 h and then was warmed to room temperature, monitored by TLC (eluent mixture: *n*-hexane/DCM 6:4). After reaction completion, saturated aqueous NH_4Cl was added until neutral pH was achieved. The organic phase was washed with brine (10 mL) and dried over sodium sulfate, filtered, and evaporated under reduced pressure. The crude was purified by flash chromatography over silica gel (eluent mixture: 8:2 *n*-hexane/EtOAc) to afford 135.1 mg of pure trisubstituted chloro alkynyl triazine amine **29** as a white solid (0.370 mmol, 86% yield). ^{1}H NMR (400 MHz, $CDCl_3$, some signals highlighted as *in the text are split due to the presence of two atropisomers in an unknown ratio): δ 7.47−7.34 (m, 4H, H biphenyl), 7.31−7.25 (m, 4H, H biphenyl), 6.33*, 5.97* (2m, 1H, NH), 5.54*, 5.47* (2s, 2H, OCH_2), 4.31−4.26 (m, 2H, NCH_2), 2.30−2.28 (m, 4H, ≡CH, CH_3). ^{13}C NMR (101 MHz, $CDCl_3$, some signals are split due to the presence of two atropisomers in an unknown ratio): δ 170.9, 166.9, 143.2, 142.0, 135.1, 133.9, 130.8, 130.6, 129.5, 129.2, 128.8, 128.2, 127.0, 125.7, 125.6, 72.4, 72.3, 69.3, 69.0, 31.2, 31.2, 29.8, 16.5, 16.4. MS (ESI$^+$) *m*/*z*: 365.35 [M + H]$^+$ calcd for $C_{20}H_{17}ClN_4O$, 364.11.

*N-(2-((4-((2-Methyl-[1,1′-biphenyl]-3-yl) methoxy)-6-(prop-2-yn-1-ylamino)-1,3,5-triazin-2-yl) amino) ethyl) Acetamide (**30**).* Trisubstituted alkynyl triazine aminoamide **30** was synthesized according to general procedure **A**, starting from intermediate **29** (135 mg, 0.370 mmol, 1 equiv), *N*-(2-aminoethyl)-acetamide (56 μL, 0.585 mmol, 1.6 equiv), and DIPEA (110 μL, 0.629 mmol, 1.7 equiv) in dry CH_3CN (5 mL) at 60 °C for 3 h. The crude was purified by flash chromatography over silica gel (eluent mixture: 95:5 DCM/MeOH) to afford 130.6 mg of pure target **30** as a white solid (0.300 mmol, 82% yield). ^{1}H NMR (400 MHz, $CDCl_3$, some signals highlighted as *in the text are split due to the presence of two atropisomers in an unknown ratio): δ 7.43−7.32 (m, 4H, H biphenyl), 7.30−7.20 (m, 4H, H biphenyl), 6.29*, 6.14*, 5.68* (3m, 3H, NH), 5.44 (m, 2H, OCH_2), 4.23 (m, 2H, NCH_2≡), 3.57, 3.43 (2m, 4H, NCH_2), 2.26−2.24 (m, 4H, CH_3, ≡CH), 1.95*, 1.93* (2s, 3H, $COCH_3$). ^{13}C NMR (101 MHz, $CDCl_3$, some signals are split due to the presence of two atropisomers in an unknown ratio): δ 170.9, 143.0, 142.1, 130.3, 129.4, 128.2, 127.0, 125.6, 40.6, 30.8, 23.4, 16.4. MS (ESI$^+$) *m*/*z*: 431.46 [M + H]$^+$ calcd for $C_{24}H_{26}N_6O_2$, 430.21.

*N-(2-Azidoethyl)-5-((3aS,4S,6aR)-2-oxohexahydro-1H-thieno[3,4-d] imidazole-4-yl) Pentanamide (**31**).* A solution of 2-azidoethanaminium chloride (139.7 mg, 1.125 mmol, 1.1 equiv) and dry DIPEA (0.827 mL, 5.115 mmol, 5 equiv) in dry DMF (2 mL) was added to a solution of biotin (250.8 mg, 1.023 mmol, 1 equiv), HOBt (414.68 mg, 3.069 mmol, 3 equiv), and EDC·HCl (586.79 mg,3.069 mmol, 3 equiv) in dry DMF (3 mL) under a nitrogen atmosphere at room temperature. The reaction mixture was stirred at room temperature for 24 h. After reaction completion (TLC monitoring, eluent mixture: 95:5 DCM/MeOH), the solvent was removed under reduced pressure. The crude was purified by Biotage reverse-phase chromatography (eluent mixture: CH_3CN/H_2O, gradient from 0% to 100% CH_3CN) to afford 234.7 mg of biotin azidoamide **31** as a white solid (0.75 mmol, 74% yield). ^{1}H NMR (400 MHz, MeOD): δ 4.49 (ddd, *J* = 7.9, 5.0, 0.8 Hz, 1H, CH), 4.30 (dd, *J* = 7.9, 4.5 Hz, 1H, CH), 3.37 (m, 4H, $NCH_2CH_2N_3$), 3.21 (ddd, *J* = 8.9, 5.8, 4.6 Hz, 1H, CHS), 2.93 (dd, *J* = 12.7, 5.0 Hz, 1H, CH_2S), 2.71 (d, *J* = 12.7 Hz, 1H, CH_2S), 2.23 (t, *J* = 7.6 Hz, 2H, CH_2CO), 1.77−1.56 (m, 4H, $SCHCH_2$, CH_2CH_2CO), 1.49−1.41 (m, 2H, $SCHCH_2CH_2$). ^{13}C NMR (101 MHz, MeOD): δ 63.4, 61.6, 57.0, 51.5, 41.0, 39.9, 36.7, 29.7, 29.5, 26.7. MS (ESI$^+$) *m*/*z*: 313.25 [M + H]$^+$; calcd MS for $C_{12}H_{20}N_6O_2S$, 312.40.

*N-(2-(4-(((4-((2-Acetamidoethyl)amino)-6-((2-methyl-[1,1′-biphenyl]-3-yl)methoxy)-1,3,5-triazin-2-yl)amino)-methyl)-1H-1,2,3-triazol-1-yl)ethyl)-5-((3aS,4S,6aR)-2-oxo-hexahydro-1H-thieno[3,4-d]imidazole-4-yl)pentanamide (**20**).* 0.5 M Aqueous solution of $CuSO_4{\cdot}5H_2O$ (77 μL) and 0.5 M aqueous solution of sodium ascorbate (58 μL) were added to a stirred solution of intermediates **30** (50.2 mg, 0.116 mmol, 1 equiv) and **31** (37.1 mg, 0.116 mmol, 1 equiv) in 1:1 THF/H_2O (1.2 mL). The resulting mixture was stirred at room temperature for 5 h, and after reaction completion (TLC monitoring, eluent mixture: 95:5 DCM/MeOH), the solvent was evaporated under reduced pressure obtaining 94.8 mg of a crude solid. The crude was purified by Biotage reverse-phase chromatography (eluent mixture: CH_3CN/H_2O, gradient from 0 to 100% CH_3CN) to afford 47.8 mg of target trisubstituted biotinylated triazine

https://doi.org/10.1021/acs.jmedchem.1c01409
J. Med. Chem. XXXX, XXX, XXX−XXX

amide **20** (0.064 mmol, 55% yield) as a white solid. ^{1}H NMR (400 MHz, DMSO-d_6, some signals highlighted as *in the text are split due to the presence of two atropisomers in an unknown ratio): δ 7.93−7.91 (m, 2H, H triazole, NH), 7.82, 7.68, 7.58 (3m, 3H, NH), 7.47−7.35 (m, 4H, H biphenyl), 7.31−7.16 (m, 4H, H biphenyl), 6.41 (m, 1H, NH biotin), 6.35 (m, 1H, NH biotin), 5.38−5.30 (m, 2H, OCH_2), 4.50−4.45 (m, 2H, $NHCH_2$-triazole), 4.37−4.34 (m, 2H, triazole-NCH_2), 4.30−4.27 (m, 1H, CH biotin), 4.12−4.10 (m, 1H, CH biotin), 3.46−3.43 (m, 2H, $CONHCH_2$-triazole), 3.29−3.26 (m, 2H, $CONHCH_2$), 3.17−3.15 (m, 2H, NCH_2), 3.07 (m, 1H, CHS), 2.80 (dd, J = 12.4, 5.1 Hz, 1H, CH_2S), 2.56 (d, J = 12.4 Hz, 1H, CH_2S), 2.18−2.16* (m, 3H, CH_3), 2.01 (m, 2H, CH_2CO), 1.79*, 1.78* (2s, 3H, $COCH_3$), 1.58 (m, 1H, $SCHCH_2$), 1.46−1.44 (m, 3H, $SCHCH_2$, CH_2CH_2CO), 1.26−1.24 (m, 2H, $SCHCH_2CH_2$). ^{13}C NMR (101 MHz, DMSO-d_6, some signals are split due to the presence of two atropisomers in an unknown ratio): δ 172.5, 169.7, 169.4, 166.8, 166.6, 162.7, 145.3, 142.1, 141.4, 135.6, 129.1, 128.2, 127.0, 125.5, 66.0, 65.7, 61.9, 59.2, 55.4, 48.6, 38.5, 35.7, 35.0, 28.1, 28.0, 25.1, 22.6, 15.8, 15.8. MS (ESI$^+$) m/z: 743.64, [M + H]$^+$; calcd for $C_{36}H_{46}N_{12}O_4S$, 742.35.

*Synthetic Procedures for Biotinylated Disubstituted triazine **21**. N-(2-((4-((2-Methyl-[1,1′-biphenyl]-3-yl)-methoxy)-1,3,5-triazin-2-yl)amino)ethyl)pent-4-ynamide (**33**).* Disubstituted alkynyl triazine amide **33** was synthesized according to general procedure **A**, starting from intermediate **25** (126.2 mg, 0.405 mmol, 1 equiv), alkynylamine **32** (68.1 mg, 0.486 mmol, 1.2 equiv), and DIPEA (212 μL, 1.215 mmol, 3 equiv) in dry THF (2.5 mL) at 70 °C for 8 h. The crude was purified by flash chromatography over silica gel (eluent mixture: 95:5 DCM/MeOH) to afford 56.2 mg of pure compound **33** as a white solid (0.190 mmol, 46% yield). ^{1}H NMR (400 MHz, $CDCl_3$, some signals highlighted as *in the text are split due to the presence of two atropisomers in an unknown ratio): δ 8.42*, 8.34* (2s, 1H, H triazine), 7.43−7.33 (m, 4H, H biphenyl), 7.30−7.23 (m, 4H, H biphenyl), 6.58*, 6.26*, 6.20*, 5.99* (4m, 2H, NH), 5.50*, 5.44* (2s, 2H, OCH_2), 3.66−3.61 (m, 2H, NCH_2), 3.53−3.49 (m, 2H, NCH_2), 2.53−2.48 (m, 2H, $\equiv CCH_2$), 2.40−2.35 (m, 2H, $COCH_2$), 2.28*, 2.26* (2s, 3H, CH_3), 1.99−1.97 (m, 1H, ≡CH). ^{13}C NMR (101 MHz, $CDCl_3$, some signals are split due to the presence of two atropisomers in an unknown ratio): δ 172.0, 143.1, 142.0, 134.8, 134.4, 130.5, 130.4, 129.5, 128.7, 128.5, 128.2, 127.0, 125.6, 69.7, 68.4, 68.0, 41.2, 40.9, 40.0, 39.6, 35.5, 16.4, 15.1. MS (ESI$^+$) m/z: 416.41, [M + H]$^+$; calcd for $C_{24}H_{25}N_5O_2$, 415.20.

*N-(2-(4-(3-((2-((4-((2-Methyl-[1,1′-biphenyl]-3-yl)-methoxy)-1,3,5-triazin-2-yl)amino)ethyl)amino)-3-oxoprop-yl)-1H-1,2,3-triazol-1-yl)ethyl)-5-((3aR,4R,6aS)-2-oxohexahy-dro-1H-thieno[3,4-d]imidazole-4-yl)pentanamide (**21**).* 0.5 M aqueous solution of $CuSO_4{\cdot}5H_2O$ (66 μL) and 0.5 M aqueous solution of sodium ascorbate (50 μL) were added to a stirred solution of intermediates **33** (41.5 mg, 0.10 mmol, 1 equiv) and **31** (31.4 mg, 0.10 mmol, 1 equiv) in 1:1 THF/H_2O (1 mL). The resulting mixture was stirred at room temperature for 5 h, and after reaction completion (TLC monitoring, eluent mixture: 95:5 DCM/MeOH), the solvent was evaporated under reduced pressure. The crude was purified by Biotage reverse-phase chromatography (eluent mixture: CH_3CN/H_2O, gradient from 0% to 100% of CH_3CN) to afford 36.0 mg of target disubstituted biotinylated amide **21** as a white amorphous solid (0.049 mmol, 49% yield). ^{1}H NMR (400 MHz, DMSO-d_6, some signals highlighted as *in the text are split due to the presence of two atropisomers in an unknown ratio): δ 8.38*, 8.28* (2s, 1H, H triazine), 8.07−7.94 (m, 3H, NH), 7.76*, 7.74* (2s, 1H, H triazole), 7.47−7.38 (m, 4H, H biphenyl), 7.33−7.18 (m, 4H, H biphenyl), 6.41 (s, 1H, NH biotin), 6.35 (s, 1H, NH biotin), 5.44*, 5.39* (2s, 2H, OCH_2), 4.35−4.28 (m, 3H, CH biotin, triazole-NCH_2), 4.13−4.10 (m, 1H, CH biotin), 3.44−3.43 (m, 2H, $CONHCH_2$-triazole), 3.23−3.16 (m, 4H, NCH_2), 3.09−3.07 (m, 1H, CHS), 2.83−2.79 (m, 3H, $COCH_2CH_2$-triazole, CH_2S), 2.57 (d, J = 12.4 Hz, 1H, CH_2S), 2.44−2.38 (m, 2H, $COCH_2CH_2$-triazole), 2.19, 2.18 (2s, 3H, CH_3), 2.03 (t, J = 7.4 Hz, 2H, $COCH_2$ biotin), 1.62−1.53 (m, 1H, $SCHCH_2$), 1.48−1.39 (m, 3H, $SCHCH_2$, CH_2CH_2CO), 1.32−1.23 (m, 2H, $SCHCH_2CH_2$). ^{13}C NMR (101 MHz, DMSO-d_6, some signals are split due to the presence of two atropisomers in an unknown ratio): δ 172.5, 171.4, 171.4, 169.7, 169.4, 167.8, 167.2, 166.5, 166.4, 162.7, 145.9, 142.2, 141.3, 134.9, 133.7, 129.8, 129.1, 128.4, 128.2, 128.0, 127.0, 125.5, 122.1, 67.4, 66.7, 61.0, 59.2, 55.4, 48.6, 38.1, 37.8, 35.5, 35.0, 28.1, 28.0, 25.1, 21.3, 15.8. MS (ESI$^+$) m/z: [M + H]$^+$, 728.62; calcd for $C_{36}H_{45}N_{11}O_4S$, 727.34.

Cell Culture, Purification of Exosomes from Cell's Supernatant, and PDL-1 Detection. Human NSCLC (A549 and H460) and breast cancer cell (BT459) lines were purchased from the ATCC. All cell lines were grown in RPMI 1640 medium (Sigma-Aldrich, Milan Italy) with 10% foetal bovine serum (Sigma-Aldrich, Milan Italy) at 37%, 5% CO2.

Purification of Exosomes and ELISA for PDL-1 Determination. Exosomes were isolated from culture media of A549, H460, and BT549 cells grown in the RPMI serum−free medium supplemented with 10% Exo free-FBS (FBS depleted of exosomes, SBI, System Biosciences) in 150 mm plates (15 mL medium volume) with Cell Culture Media Exosome Purification Media Kits (Norgen, Biotek Corp). Briefly, 20 mL of the cell supernatant was centrifuged at 200*g* for 15 min to remove cell debris and then processed according to the manufacturer's instruction.[64]

For PD-L1 determination, 4*v*g of A549, BT-549, and H460 exomes were coated on an ELISA high binding plate (Greiner Bio-One, Sigma Aldrich) overnight. After 24 h, the plate was incubated with BSA 3% in PBS for 2hr. An anti-PD-L1 primary antibody (1:400 H130-sc50298, Santacruz Biotechnology) in 1% BSA in PBS was incubated for 1 h at room temperature. Then, the plate was washed three times with 300 μL of PBS, and a secondary HRP antibody (Immunoreagents) 1:2000 in BSA 1% PBS was incubated 1 h at room temperature. Afterward, the plate was washed three times before the addition of a 3,3,5,5-tetramethylbenzidine substrate solution. The reaction was stopped with 0.16 M sulfuric acid. The signal intensity was analyzed by measuring the absorbance at 450 nm with a microplate reader (Thermo Fisher Scientific).

■ ASSOCIATED CONTENT

Supporting Information

The Supporting Information is available free of charge at https://pubs.acs.org/doi/10.1021/acs.jmedchem.1c01409.

^{1}H-1D NMR spectrum of hPD-L1 in the absence and in the presence of **7**−**22**, inhibition curves (IC_{50}) of **10**−**11**, **13**−**17**, and **BMS-202**, DSC profiles for PD-L1 in the absence and the presence of **10** and **BMS-202**, docking-predicted binding pose of **14** in the homodimeric PD-L1 binding site, *in vitro* antitumor effect of **10**, ELISA assay performed on isolated whole exosome, 1H NMR, 13C NMR spectra, and HPLC chromatograms of the

synthesized compounds, synthesis of the negative control (compound **22**), physicochemical properties prediction of **1**, **5**, and **10**, and supplementary references (PDF)
Molecular formula strings (CSV)

AUTHOR INFORMATION

Corresponding Authors

Francesco Sabbatino − *Dipartimento di Medicina e Chirurgia, Ospedale "San Giovanni di Dio e Ruggi d'Aragona", Università di Salerno, Salerno 84131, Italy*; Email: fsabbatino@unisa.it

Pierfausto Seneci − *Chemistry Department, Università degli Studi di Milano, Milan 20133, Italy*; orcid.org/0000-0001-9709-7344; Email: pierfausto.seneci@unimi.it

Daniela Arosio − *Istituto di Scienze e Tecnologie Chimiche "Giulio Natta" (SCITEC), Consiglio Nazionale delle Ricerche (CNR), Milan 20133, Italy*; Email: daniela.arosio@scitec.cnr.it

Luciana Marinelli − *Dipartimento di Farmacia, Università degli Studi di Napoli Federico II, Napoli 80131, Italy*; orcid.org/0000-0002-4084-8044; Email: lmarinel@unina.it

Authors

Pasquale Russomanno − *Dipartimento di Farmacia, Università degli Studi di Napoli Federico II, Napoli 80131, Italy*

Giulia Assoni − *Department of Cellular, Computational and Integrative Biology, (CIBIO), Università degli Studi di Trento, Povo I-38123 Trento, Italy; Chemistry Department, Università degli Studi di Milano, Milan 20133, Italy*

Jussara Amato − *Dipartimento di Farmacia, Università degli Studi di Napoli Federico II, Napoli 80131, Italy*; orcid.org/0000-0001-6096-3544

Vincenzo Maria D'Amore − *Dipartimento di Farmacia, Università degli Studi di Napoli Federico II, Napoli 80131, Italy*

Riccardo Scaglia − *Chemistry Department, Università degli Studi di Milano, Milan 20133, Italy*

Diego Brancaccio − *Dipartimento di Farmacia, Università degli Studi di Napoli Federico II, Napoli 80131, Italy*

Martina Pedrini − *Chemistry Department, Università degli Studi di Milano, Milan 20133, Italy*

Giovanna Polcaro − *Dipartimento di Medicina e Chirurgia, Ospedale "San Giovanni di Dio e Ruggi d'Aragona", Università di Salerno, Salerno 84131, Italy*

Valeria La Pietra − *Dipartimento di Farmacia, Università degli Studi di Napoli Federico II, Napoli 80131, Italy*

Paolo Orlando − *Chemistry Department, Università degli Studi di Milano, Milan 20133, Italy*

Marianna Falzoni − *Chemistry Department, Università degli Studi di Milano, Milan 20133, Italy*

Linda Cerofolini − *Centro di Risonanza Magnetica, CERM, Università di Firenze, Firenze 50019, Italy*

Stefano Giuntini − *Centro di Risonanza Magnetica, CERM, Università di Firenze, Firenze 50019, Italy*

Marco Fragai − *Centro di Risonanza Magnetica, CERM, Università di Firenze, Firenze 50019, Italy*; orcid.org/0000-0002-8440-1690

Bruno Pagano − *Dipartimento di Farmacia, Università degli Studi di Napoli Federico II, Napoli 80131, Italy*; orcid.org/0000-0002-7716-9010

Greta Donati − *Dipartimento di Farmacia, Università degli Studi di Napoli Federico II, Napoli 80131, Italy*

Ettore Novellino − *Università Cattolica del Sacro Cuore, Rome 00168, Italy*; orcid.org/0000-0002-2181-2142

Cristina Quintavalle − *Department of Molecular Medicine and Medical Biotechnology, "Federico II" University, Naples, Italy; Institute for Experimental Endocrinology and Oncology (IEOS), National Research Council (CNR), Naples 80131, Italy*

Gerolama Condorelli − *Department of Molecular Medicine and Medical Biotechnology, "Federico II" University, Naples, Italy; Institute for Experimental Endocrinology and Oncology (IEOS), National Research Council (CNR), Naples 80131, Italy; Department of Molecular Medicine and Medical Biotechnology, "Federico II" University, Naples 80131, Italy*

Stefano Pepe − *Dipartimento di Medicina e Chirurgia, Ospedale "San Giovanni di Dio e Ruggi d'Aragona", Università di Salerno, Salerno 84131, Italy*

Complete contact information is available at: https://pubs.acs.org/10.1021/acs.jmedchem.1c01409

Author Contributions

P.R., G.A., and J.A. equally contributed to the work. The manuscript was written through contributions of all authors. All authors have given approval to the final version of the manuscript.

Funding

This research was funded by the Italian Ministry of Education, University, and Research (MIUR), Progetti di Rilevante Interesse Nazionale (PRIN) 2017 (2017PHRC8X 004). We also acknowledge Regione Campania—POR Campania FESR 2014/2020 (B61G18000470007). H2020-MSCA-RISE-2019 cONCReTE (872391), H2020-MSCA-RISE-2019 PRISAR2 (872860), MSCA-ITN-ETN CAST (857894), MSCA-ITN-ETN PAVE (861190), and Regione Campania Project PO FESR 2014-2020-SATIN.

Notes

The authors declare no competing financial interest.

ACKNOWLEDGMENTS

Dedicated to Leonardo Manzoni, a friend and a colleague, who was instrumental for the success of our work.

REFERENCES

(1) Balkwill, F.; Mantovani, A. Inflammation and Cancer: Back to Virchow? *Lancet* **2001**, *357*, 539−545.

(2) Chen, G.; Huang, A. C.; Zhang, W.; Zhang, G.; Wu, M.; Xu, W.; Yu, Z.; Yang, J.; Wang, B.; Sun, H.; Xia, H.; Man, Q.; Zhong, W.; Antelo, L. F.; Wu, B.; Xiong, X.; Liu, X.; Guan, L.; Li, T.; Liu, S.; Yang, R.; Lu, Y.; Dong, L.; McGettigan, S.; Somasundaram, R.; Radhakrishnan, R.; Mills, G.; Lu, Y.; Kim, J.; Chen, Y. H.; Dong, H.; Zhao, Y.; Karakousis, G. C.; Mitchell, T. C.; Schuchter, L. M.; Herlyn, M.; Wherry, E. J.; Xu, X.; Guo, W. Exosomal PD-L1 Contributes to Immunosuppression and Is Associated with Anti-PD-1 Response. *Nature* **2018**, *560*, 382−386.

(3) Qin, S.; Xu, L.; Yi, M.; Yu, S.; Wu, K.; Luo, S. Novel Immune Checkpoint Targets: Moving beyond PD-1 and CTLA-4. *Mol. Cancer* **2019**, *18*, 155−14.

(4) Kim, D. H.; Kim, H.; Choi, Y. J.; Kim, S. Y.; Lee, J.-E.; Sung, K. J.; Sung, Y. H.; Pack, C.-G.; Jung, M.-k.; Han, B.; Kim, K.; Kim, W. S.; Nam, S. J.; Choi, C.-M.; Yun, M.; Lee, J. C.; Rho, J. K. Exosomal PD-L1 Promotes Tumor Growth through Immune Escape in Non-Small Cell Lung Cancer. *Exp. Mol. Med.* **2019**, *51*, 1−13.

(5) Theodoraki, M.-N.; Yerneni, S. S.; Hoffmann, T. K.; Gooding, W. E.; Whiteside, T. L. Clinical Significance of PD-L1+ Exosomes in Plasma of Head and Neck Cancer Patients. *Clin. Cancer Res.* **2018**, *24*, 896−905.

(6) Fan, Y.; Che, X.; Qu, J.; Hou, K.; Wen, T.; Li, Z.; Li, C.; Wang, S.; Xu, L.; Liu, Y.; Qu, X. Exosomal PD-L1 Retains Immunosuppressive Activity and Is Associated with Gastric Cancer Prognosis. *Ann. Surg Oncol.* **2019**, *26*, 3745−3755.

(7) Poole, R. M. Pembrolizumab: First Global Approval. *Drugs* **2014**, *74*, 1973−1981.

(8) Wang, C.; Thudium, K. B.; Han, M.; Wang, X.-T.; Huang, H.; Feingersh, D.; Garcia, C.; Wu, Y.; Kuhne, M.; Srinivasan, M.; Singh, S.; Wong, S.; Garner, N.; Leblanc, H.; Bunch, R. T.; Blanset, D.; Selby, M. J.; Korman, A. J. Vitro Characterization of the Anti-PD-1 Antibody Nivolumab, BMS-936558, and in Vivo Toxicology in Non-Human Primates. *Cancer Immunol. Res.* **2014**, *2*, 846−856.

(9) Ribas, A.; Wolchok, J. D. Cancer Immunotherapy Using Checkpoint Blockade. *Science* **2018**, *359*, 1350−1355.

(10) Antonia, S. J.; Villegas, A.; Daniel, D.; Vicente, D.; Murakami, S.; Hui, R.; Yokoi, T.; Chiappori, A.; Lee, K. H.; de Wit, M.; Cho, B. C.; Bourhaba, M.; Quantin, X.; Tokito, T.; Mekhail, T.; Planchard, D.; Kim, Y.-C.; Karapetis, C. S.; Hiret, S.; Ostoros, G.; Kubota, K.; Gray, J. E.; Paz-Ares, L.; de Castro Carpeño, J.; Wadsworth, C.; Melillo, G.; Jiang, H.; Huang, Y.; Dennis, P. A.; Özgüroğlu, M. Durvalumab after Chemoradiotherapy in Stage III Non-Small-Cell Lung Cancer. *N. Engl. J. Med.* **2017**, *377*, 1919−1929.

(11) Joseph, J.; Zobniw, C.; Davis, J.; Anderson, J.; Trinh, V. A. Avelumab: A Review of Its Application in Metastatic Merkel Cell Carcinoma. *Ann. Pharmacother.* **2018**, *52*, 928−935.

(12) Sullivan, R. J.; Flaherty, K. T. Anti-PD-1 therapies-a new first-line option in advanced melanoma. *Nat. Rev. Clin. Oncol.* **2015**, *12*, 625−626.

(13) Khanna, P.; Blais, N.; Gaudreau, P.-O.; Corrales-Rodriguez, L. Immunotherapy Comes of Age in Lung Cancer. *Clin. Lung Cancer* **2017**, *18*, 13−22.

(14) Lee, C. M.; Tannock, I. F. The Distribution of the Therapeutic Monoclonal Antibodies Cetuximab and Trastuzumab within Solid Tumors. *BMC Cancer* **2010**, *10*, 255.

(15) Wargo, J. A.; Reuben, A.; Cooper, Z. A.; Oh, K. S.; Sullivan, R. J. Immune Effects of Chemotherapy, Radiation, and Targeted Therapy and Opportunities for Combination With Immunotherapy. *Semin. Oncol.* **2015**, *42*, 601−616.

(16) Miller, M. M.; Mapelli, C.; Allen, M.; Bowsher, M. S.; Boy, K.; Gillis, E. Macrocyclic Inhibitors of the Pd-1/Pd-L1 and Cd80(B7-1)/Pd-L1 Protein/Protein Interactions. Patent WO 2014151634 A1, 2014.

(17) Chupak, L.; Zheng, X. Compounds Useful as Immunomodulators. Patent WO 2015034820 A1, 2015.

(18) Chupak, L. S.; Ding, M.; Martin, S. W.; Zheng, X.; Hewawasam, P.; Connoly, T. P.; Xu, N.; Yeung, K. S.; Zhu, J.; Langley, D. R.; Tenney, D. J., S. P. Compounds Useful as Immunomodulators. Patent Appl. WO 2015160641 A2, 2015.

(19) Miller, M. M.; Mapelli, C.; Allen, A. P.; Bowsher, M. S.; Gillis, E. P.; Langley, D. R.; Mull, E.; Poirier, M. A.; Sanghvi, N.; Sun, l.-Q.; Tenney, D. J.; Yeung, K.-S.; Zhu, J.; Gillman, K. W.; Zhao, Q.; Grant-Young, K. A.; Scola, P. M.; Cornelius, l. A. M. Macrocyclic Inhibitors of the Pd-1/Pd-L1 and Cd80 (B7-1)/Pd-L1 Protein/Protein Interactions. Patent Appl. WO 2016039749 A1, 2016.

(20) Zarganes-Tzitzikas, T.; Konstantinidou, M.; Gao, Y.; Krzemien, D.; Zak, K.; Dubin, G.; Holak, T. A.; Dömling, A. Inhibitors of Programmed Cell Death 1 (PD-1): A Patent Review (2010-2015). *Expert Opin. Ther. Pat.* **2016**, *26*, 973−977.

(21) Magiera-Mularz, K.; Skalniak, L.; Zak, K. M.; Musielak, B.; Rudzinska-Szostak, E.; Berlicki, Ł.; Kocik, J.; Grudnik, P.; Sala, D.; Zarganes-Tzitzikas, T.; Shaabani, S.; Dömling, A.; Dubin, G.; Holak, T. A. Bioactive Macrocyclic Inhibitors of the PD-1/PD-L1 Immune Checkpoint. *Angew. Chem. Int. Ed.* **2017**, *56*, 13732−13735.

(22) Guzik, K.; Zak, K. M.; Grudnik, P.; Magiera, K.; Musielak, B.; Törner, R.; Skalniak, L.; Dömling, A.; Dubin, G.; Holak, T. A. Small-Molecule Inhibitors of the Programmed Cell Death-1/Programmed Death-Ligand 1 (PD-1/PD-L1) Interaction via Transiently Induced Protein States and Dimerization of PD-L1. *J. Med. Chem.* **2017**, *60*, 5857−5867.

(23) Konstantinidou, M.; Zarganes-Tzitzikas, T.; Magiera-Mularz, K.; Holak, T. A.; Dömling, A. Immune Checkpoint PD-1/PD-L1: Is There Life Beyond Antibodies? *Angew. Chem. Int. Ed.* **2018**, *57*, 4840−4848.

(24) Kopalli, S. R.; Kang, T.-B.; Lee, K.-H.; Koppula, S. Novel Small Molecule Inhibitors of Programmed Cell Death (PD)-1, and Its Ligand, PD-L1 in Cancer Immunotherapy: A Review Update of Patent Literature. *Recent Pat. Anticancer. Drug Discov.* **2019**, *14*, 100−112.

(25) Basu, S.; Yang, J.; Xu, B.; Magiera-Mularz, K.; Skalniak, L.; Musielak, B.; Kholodovych, V.; Holak, T. A.; Hu, L. Design, Synthesis, Evaluation, and Structural Studies of C2-Symmetric Small Molecule Inhibitors of Programmed Cell Death-1/Programmed Death-Ligand 1 Protein-Protein Interaction. *J. Med. Chem.* **2019**, *62*, 7250−7263.

(26) Guzik, K.; Tomala, M.; Muszak, D.; Konieczny, M.; Hec, A.; Błaszkiewicz, U.; Pustuła, M.; Butera, R.; Dömling, A.; Holak, T. A. Development of the Inhibitors That Target the PD-1/PD-L1 Interaction—A Brief Look at Progress on Small Molecules, Peptides and Macrocycles. *Molecules* **2019**, *24*, 1−30.

(27) Wang, T.; Wu, X.; Guo, C.; Zhang, K.; Xu, J.; Li, Z.; Jiang, S. Development of Inhibitors of the Programmed Cell Death-1/Programmed Cell Death-Ligand 1 Signaling Pathway. *J. Med. Chem.* **2019**, *62*, 1715−1730.

(28) Cheng, B.; Xiao, Y.; Xue, M.; Cao, H.; Chen, J. Recent Advances in the Development of PD-L1 Modulators: Degraders, Downregulators, and Covalent Inhibitors. *J. Med. Chem.* **2020**, *63*, 15389−15398.

(29) Cheng, B.; Ren, Y.; Niu, X.; Wang, W.; Wang, S.; Tu, Y.; Liu, S.; Wang, J.; Yang, D.; Liao, G.; Chen, J. Discovery of Novel Resorcinol Dibenzyl Ethers Targeting the Programmed Cell Death-1/Programmed Cell Death-Ligand 1 Interaction as Potential Anticancer Agents. *J. Med. Chem.* **2020**, *63*, 8338−8358.

(30) Cheng, B.; Wang, W.; Niu, X.; Ren, Y.; Liu, T.; Cao, H.; Wang, S.; Tu, Y.; Chen, J.; Liu, S.; Yang, X.; Chen, J. Discovery of Novel and Highly Potent Resorcinol Dibenzyl Ether-Based PD-1/PD-L1 Inhibitors with Improved Drug-like and Pharmacokinetic Properties for Cancer Treatment. *J. Med. Chem.* **2020**, *63*, 15946−15959.

(31) Guo, J.; Luo, L.; Wang, Z.; Hu, N.; Wang, W.; Xie, F.; Liang, E.; Yan, X.; Xiao, J.; Li, S. Design, Synthesis, and Biological Evaluation of Linear Aliphatic Amine-Linked Triaryl Derivatives as Potent Small-Molecule Inhibitors of the Programmed Cell Death-1/Programmed Cell Death-Ligand 1 Interaction with Promising Antitumor Effects in Vivo. *J. Med. Chem.* **2020**, *63*, 13825−13850.

(32) Li, S.; Vilalta-Colomer, M.; Punna, S.; Malathong, V.; Singh, R.; Zhang, P. Preparation of Small Molecule Programmed Death Ligand 1 Phenylindanyloxybenzylamines Including N-(Phenylindanyloxybenzyl)-Amino Acid Derivatives, and Methods of Treating Cancer Using Them. Patent Appl. WO 2020047035 A1, 2020.

(33) Konieczny, M.; Musielak, B.; Kocik, J.; Skalniak, L.; Sala, D.; Czub, M.; Magiera-Mularz, K.; Rodriguez, I.; Myrcha, M.; Stec, M.; Siedlar, M.; Holak, T. A.; Plewka, J. Di-Bromo-Based Small-Molecule Inhibitors of the PD-1/PD-L1 Immune Checkpoint. *J. Med. Chem.* **2020**, *63*, 11271−11285.

(34) Narva, S.; Xiong, X.; Ma, X.; Tanaka, Y.; Wu, Y.; Zhang, W. Synthesis and Evaluation of Biphenyl-1,2,3-Triazol-Benzonitrile Derivatives as PD-1/PD-L1 Inhibitors. *ACS Omega* **2020**, *5*, 21181−21190.

(35) Qin, M.; Cao, Q.; Zheng, S.; Tian, Y.; Zhang, H.; Xie, J.; Xie, H.; Liu, Y.; Zhao, Y.; Gong, P. Discovery of [1,2,4]Triazolo[4,3-a]pyridines as Potent Inhibitors Targeting the Programmed Cell Death-1/Programmed Cell Death-Ligand 1 Interaction. *J. Med. Chem.* **2019**, *62*, 4703−4715.

(36) Zhang, Y.; Denhg, J.; Feng, Z.; Jiang, L.; Lu, X.; Shang, K.; Shou, J.; Wang, B.; Xu, X.; Xu, Y. Preparation and Application of Class of N-Containing Heterocyclic Compounds Having Immunoregulatory Function. Patent Appl. WO 2020024997 A1, 2020.

(37) Zhang, Y.; Deng, J.; Feng, Z.; Huang, L.; Jiang, L.; Lu, X.; Shang, K.; Shou, J.; Wang, B.; Xu, X.; Xu, Y. Preparation and Application of Aromatic Compound Having Immunoregulatory Function. Patent Appl. WO2020025030 A1, 2020.

(38) Zak, K. M.; Kitel, R.; Przetocka, S.; Golik, P.; Guzik, K.; Musielak, B.; Dömling, A.; Dubin, G.; Holak, T. A. Structure of the Complex of

https://doi.org/10.1021/acs.jmedchem.1c01409
J. Med. Chem. XXXX, XXX, XXX−XXX

Human Programmed Death 1, PD-1, and Its Ligand PD-L1. *Structure* **2015**, *23*, 2341−2348.

(39) Zak, K. M.; Grudnik, P.; Guzik, K.; Zieba, B. J.; Musielak, B.; Dömling, A.; Dubin, G.; Holak, T. A. Structural Basis for Small Molecule Targeting of the Programmed Death Ligand 1 (PD-L1). *Oncotarget* **2016**, *7*, 30323−30335.

(40) Skalniak, L.; Zak, K. M.; Guzik, K.; Magiera, K.; Musielak, B.; Pachota, M.; Szelazek, B.; Kocik, J.; Grudnik, P.; Tomala, M.; Krzanik, S.; Pyrc, K.; Dömling, A.; Dubin, G.; Holak, T. A. Small-Molecule Inhibitors of PD-1/PD-L1 Immune Checkpoint Alleviate the PD-L1-Induced Exhaustion of T-Cells. *Oncotarget* **2017**, *8*, 72167−72181.

(41) Amaral, M.; Kokh, D. B.; Bomke, J.; Wegener, A.; Buchstaller, H. P.; Eggenweiler, H. M.; Matias, P.; Sirrenberg, C.; Wade, R. C.; Frech, M. Protein Conformational Flexibility Modulates Kinetics and Thermodynamics of Drug Binding. *Nat. Commun.* **2017**, *8*, 2276.

(42) Perry, E.; Mills, J. J.; Zhao, B.; Wang, F.; Sun, Q.; Christov, P. P.; Tarr, J. C.; Rietz, T. A.; Olejniczak, E. T.; Lee, T.; Fesik, S. Fragment-Based Screening of Programmed Death Ligand 1 (PD-L1). *Bioorg. Med. Chem. Lett.* **2019**, *29*, 786−790.

(43) Cheng, B.; Yuan, W.-E.; Su, J.; Liu, Y.; Chen, J. Recent Advances in Small Molecule Based Cancer Immunotherapy. *Eur. J. Med. Chem.* **2018**, *157*, 582−598.

(44) Hu, Z.; Yu, P.; Du, G.; Wang, W.; Zhu, H.; Li, N.; Zhao, H.; Dong, Z.; Ye, L.; Tian, J. PCC0208025 (BMS202), a Small Molecule Inhibitor of PD-L1, Produces an Antitumor Effect in B16-F10 Melanoma-Bearing Mice. *PLoS One* **2020**, *15*, No. e0228339.

(45) Magiera-Mularz, K.; Kocik, J.; Musielak, B.; Plewka, J.; Sala, D.; Machula, M.; Grudnik, P.; Hajduk, M.; Czepiel, M.; Siedlar, M.; Holak, T. A.; Skalniak, L. Human and Mouse PD-L1: Similar Molecular Structure, but Different Druggability Profiles. *iScience* **2021**, *24*, 101960.

(46) Sharma, A.; El-Faham, A.; de la Torre, B. G.; Albericio, F. Exploring the Orthogonal Chemoselectivity of 2,4,6-Trichloro-1,3,5-Triazine (TCT) as a Trifunctional Linker with Different Nucleophiles: Rules of the Game. *Front. Chem.* **2018**, *6*, 516.

(47) Naseer, M. M.; Wang, D.-X.; Zhao, L.; Huang, Z.-T.; Wang, M.-X. Synthesis and Functionalization of Heteroatom-Bridged Bicyclocalixaromatics, Large Molecular Triangular Prisms with Electron-Rich and -Deficient Aromatic Interiors. *J. Org. Chem.* **2011**, *76*, 1804−1813.

(48) Sartori, A.; Portioli, E.; Battistini, L.; Calorini, L.; Pupi, A.; Vacondio, F.; Arosio, D.; Bianchini, F.; Zanardi, F. Synthesis of Novel c(AmpRGD)-Sunitinib Dual Conjugates as Molecular Tools Targeting the $\alpha v\beta 3$ Integrin/VEGFR2 Couple and Impairing Tumor-Associated Angiogenesis. *J. Med. Chem.* **2017**, *60*, 248−262.

(49) Krell, T.; Maclean, J.; Boam, D. J.; Cooper, A.; Resmini, M.; Brocklehurst, K.; Kelly, S. M.; Price, N. C.; Lapthorn, A. J.; Coggins, J. R. Biochemical and X-Ray Crystallographic Studies on Shikimate Kinase: The Important Structural Role of the P-Loop Lysine. *Protein Sci.* **2001**, *10*, 1137−1149.

(50) Anastasiadou, E.; Slack, F. J. Malicious Exosomes. *Science* **2014**, *346*, 1459−1460.

(51) Sahebi, R.; Langari, H.; Fathinezhad, Z.; Bahari Sani, Z.; Avan, A.; Ghayour Mobarhan, M.; Rezayi, M. Exosomes: New Insights into Cancer Mechanisms. *J. Cell. Biochem.* **2020**, *121*, 7−16.

(52) Yang, Y.; Li, C.-W.; Chan, L.-C.; Wei, Y.; Hsu, J.-M.; Xia, W.; Cha, J.-H.; Hou, J.; Hsu, J. L.; Sun, L.; Hung, M.-C. Exosomal PD-L1 Harbors Active Defense Function to Suppress t Cell Killing of Breast Cancer Cells and Promote Tumor Growth. *Cell Res.* **2018**, *28*, 862−864.

(53) Zhou, K.; Guo, S.; Li, F.; Sun, Q.; Liang, G. Exosomal PD-L1: New Insights Into Tumor Immune Escape Mechanisms and Therapeutic Strategies. *Front. Cell Dev. Biol.* **2020**, *8*, 569219−19.

(54) Mayer, M.; Meyer, B. Characterization of Ligand Binding by Saturation Transfer Difference NMR Spectroscopy. *Angew. Chem. Int. Ed.* **1999**, *38*, 1784−1788.

(55) Dalvit, C.; Fogliatto, G.; Stewart, A.; Veronesi, M.; Stockman, B. WaterLOGSY as a Method for Primary NMR Screening: Practical Aspects and Range of Applicability. *J. Biomol. NMR* **2001**, *21*, 349−359.

(56) Meyer, B.; Peters, T. NMR Spectroscopy Techniques for Screening and Identifying Ligand Binding to Protein Receptors. *Angew. Chem. Int. Ed.* **2003**, *42*, 864−890.

(57) Hwang, T. L.; Shaka, A. J. Water Suppression That Works. Excitation Sculpting Using Arbitrary Wave-Forms and Pulsed-Field Gradients. *J. Magn. Reson., Ser. A* **1995**, *112*, 275−279.

(58) Shelley, J. C.; Cholleti, A.; Frye, L. L.; Greenwood, J. R.; Timlin, M. R.; Uchimaya, M. Epik: a software program for pK a prediction and protonation state generation for drug-like molecules. *J. Comput. Aided Mol. Des.* **2007**, *21*, 681−691.

(59) Greenwood, J. R.; Calkins, D.; Sullivan, A. P.; Shelley, J. C. Towards the Comprehensive, Rapid, and Accurate Prediction of the Favorable Tautomeric States of Drug-like Molecules in Aqueous Solution. *J. Comput. Aided Mol. Des.* **2010**, *24*, 591−604.

(60) Madhavi Sastry, G.; Adzhigirey, M.; Day, T.; Annabhimoju, R.; Sherman, W. Protein and Ligand Preparation: Parameters, Protocols, and Influence on Virtual Screening Enrichments. *J. Comput. Aided Mol. Des.* **2013**, *27*, 221−234.

(61) Friesner, R. A.; Banks, J. L.; Murphy, R. B.; Halgren, T. A.; Klicic, J. J.; Mainz, D. T.; Repasky, M. P.; Knoll, E. H.; Shelley, M.; Perry, J. K.; Shaw, D. E.; Francis, P.; Shenkin, P. S. Glide: A New Approach for Rapid, Accurate Docking and Scoring. 1. Method and Assessment of Docking Accuracy. *J. Med. Chem.* **2004**, *47*, 1739−1749.

(62) Halgren, T. A.; Murphy, R. B.; Friesner, R. A.; Beard, H. S.; Frye, L. L.; Pollard, W. T.; Banks, J. L. Glide: A New Approach for Rapid, Accurate Docking and Scoring. 2. Enrichment Factors in Database Screening. *J. Med. Chem.* **2004**, *47*, 1750−1759.

(63) Harder, E.; Damm, W.; Maple, J.; Wu, C.; Reboul, M.; Xiang, J. Y.; Wang, L.; Lupyan, D.; Dahlgren, M. K.; Knight, J. L.; Kaus, J. W.; Cerutti, D. S.; Krilov, G.; Jorgensen, W. L.; Abel, R.; Friesner, R. A. OPLS3: A Force Field Providing Broad Coverage of Drug-like Small Molecules and Proteins. *J. Chem. Theory Comput.* **2016**, *12*, 281−296.

(64) Esposito, C. L.; Quintavalle, C.; Ingenito, F.; Rotoli, D.; Roscigno, G.; Nuzzo, S.; Thomas, R.; Catuogno, S.; de Franciscis, V.; Condorelli, G. Identification of a Novel RNA Aptamer That Selectively Targets Breast Cancer Exosomes. *Mol. Ther. Nucleic Acids* **2021**, *23*, 982−994.

https://doi.org/10.1021/acs.jmedchem.1c01409
J. Med. Chem. XXXX, XXX, XXX−XXX